MELT PROCESSING OF $SmBa_2Cu_3O_y$

SUPERCONDUCTOR : A STUDY OF

MICROSTRUCTURE AND MAGNETIC PROPERTIES

A THESIS SUBMITTED FOR THE DEGREE OF
DOCTOR OF PHILOSOPHY

BY

N. V. N. Viswanath

SCHOOL OF PHYSICS
UNIVERSITY OF HYDERABAD
HYDERABAD - 500 046 INDIA
NOVEMBER 1997

DEDICATED
TO
MY PARENTS

CERTIFICATE

This is to certify that the research work compiled in this thesis entitled "MELT PROCESSING OF SmBa$_2$Cu$_3$O$_y$ SUPERCONDUCTOR : A STUDY OF MICROSTRUCTURE AND MAGNETIC PROPERTIES" has been carried out by Mr. N. V. N. Viswanath under my supervision and the same has not been submitted for the award of any degree of any University.

Date   :   3-11-97
Place : Hyderabad

Dr. T. RAJASEKHARAN
RESEARCH SUPERVISOR

DEAN
SCHOOL OF PHYSICS

DEAN,
SCHOOL OF PHYSICS,
UNIVERSITY OF HYDERABAD.

ACKNOWLEDGEMENTS

DECLARATION

I hereby declare that the work reported in this thesis has been carried out by me under supervision of Dr. T. Rajasekharan at Defence Metallurgical Research Laboratory (DMRL), Hyderabad. I also declare that this has not been submitted to any University or Institution for the award of any degree/diploma.

Date :   3-11-97   **N.V.N.Viswanath**
Place : Hyderabad

CONTENTS

CHAPTER I

<u>INTRODUCTION</u>

In 1911, Kamerlingh Onnes discovered superconductivity in Mercury at 4.2 K. Since then superconductivity had been discovered in many compounds and **with** increasing transition temperature (T_c). A major breakthrough occurred in 1986, when **Bednorz** & Muller [1] discovered superconductivity in La-Ba-Cu-0 around 35 K. This discovery opened the field of high temperature superconductivity. Later, Chu & Wu [2] discovered the first material capable of becoming superconducting above liquid nitrogen temperature. The material was $YBa_2Cu_3O_x$, with a T_c above 90 K. **Following** this, three families of superconducting compounds were discovered with even higher values of T_c. Maeda **[3]** found superconductivity in Bi-Sr-Ca-Cu-O system with a maximum T_c of 110 K. Herman |4] observed superconductivity **in** the Tl-Ba-Ca-Cu-O system with a T_c of 125 K. Putillin *el al*. [5] discovered superconductivity in Hg-Ba-Ca-Cu-0 system with a T_c of 136 K.

Neutron diffraction experiments determined the structure of the high-T_c compounds to be tetragonal **for** La-Ba-Cu-0 system and orthorhombic for all the other compounds. The Y- compound has a pervoskite structure and the Bi-, Tl- & Hg- systems have layered structures. It is possible to obtain a series of layered compounds with varying stoichiometry by varying numbers of Cu-0 planes into the unit cell. For each new Cu-0 plane an adjacent Ca-0 plane is also introduced. The general formula is $B_x A_2 Ca_{n-1} Cu_n O_x$, where B is Bi, Tl or Hg, A is Sr for Bi,

Ba for Tl, Hg compounds. n is the number of Cu-O layers per unit cell, which can take values from 1 to 4. The subscript y is 1 or 2, denoting single or double layers. By increasing n, the T_c rises. 1; is difficult to obtain a single phase of these layered compounds, a mixture of phases is usually observed. The Y-compound is a line compound and a single phase is observed.

The La-, Bi-, & Tl- compounds have planes of Cu and O atoms, and the Y-compounds have both planes and chains of Cu and O atoms [6]. The structure of it is shown in Fig. 1.1. The planes play the role in generating superconductivity and chains act as electron reservoirs which can be filled or emptied by changing the oxygen stoichiometry or by doping [7]. In Y-system, with the reduction in number of oxygen atoms per formula unit, the T_c decreases to below 50 K. The Y-system exhibits twinning and it was speculated that the twin planes **are a** source of superconductivity , but it **was** latter disproved because the other systems like Bi-, T1-, & Hg- do not exhibit twinning and are nevertheless superconducting. Soon it was realized that any rare-earth can be replaced at the Y-site and the compound will have the same T_c same as the Y-compound, except for Ce, Pr and La.

Sintering is a common ceramic processing technique and **the high-T_c** compounds were prepared by the solid state sintering route. Soon **it** was realized that eventhough the T_c values were good, the current density values were too low to be useful in practical applications [8J. Thin film deposition of these compound was done, which gave good values of J_c. This technique cannot be useful where samples in bulk form are needed like in superconducting magnets, bearings, flywheels, **fault** current limiters, etc,. In the sintered samples the factors limiting J_c are the anisotropic grain growth, grain boundary weak links and lack of effective

pinning centers. Alignment of the grains is an answer for increasing the J_c. Melt

processing of Y-123 system has opened the possibility of overcoming all these

difficulties and obtaining high J_c.
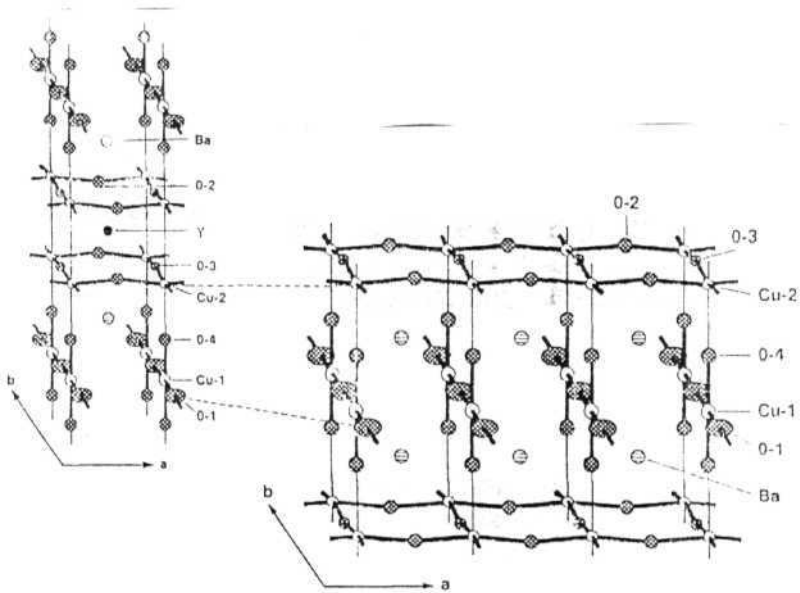
Fig. 1.1 : Crystal structure of 123. showing the CuO planes and chains.

1.1. MELT TEXTURING

Jin *et al,* [9] were the first to report the texturing of Y-123 by melt processing. It was done by following the pseudo binary phase diagram of the 123 system, as shown in Fig. 1.2. The 123 phase peritectically dissociates above 1010°C to form solid Y_2BaCuO_5 and liquid phases (L1) according to the reaction :

$$2YBa_2Cu_3O_x \leftrightarrow Y_2BaCuO_5 + L1 \ (3 \ BaCuO_3 + 2 \ CuO) \qquad 1010^{\circ}C \ to \ 1200^{\circ}C$$
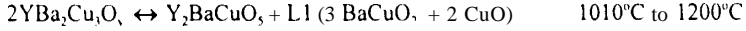
At higher temperatures the Y_2BaCuO_5 dissociates into Y_2O_3 and liquid phase (L2)

$$Y_2BaCuO_5 \rightarrow Y_2O_3 + L2 \ (\ BaO + CuO) \qquad 1200^{\circ}C \ to \ 1500^{\circ}C$$
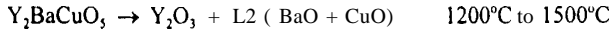
Jin *el al.* [9] melted Y-123 sample at 1300°C ant cooled it at a rate of 5°C/hr to room temperature. This was called the melt textured growth process (MTG). where the sample was melted above the peritectic decomposition temperature (T_p) to form 211 & liquid phases. This semi solid melt is slow cooled from T_p, where the 211 phase reacts with the liquid phases to form 123. The microstructure of the sample showed aligned grains in the ab-plane, with Y-211 particles distributed in the 123 grains. Due to the alignment of the grains the sample had a J_c of 10^4 amp/cnr at 77 K. Salama *el al.* [10] modified the MTG process by changing the operating temperatures and cooling rates. They avoided going to higher temperatures above the 211 + liquid phase region, but kept above T_p for a brief period (10 to 20 minutes), and immediately decreased to the peritectic temperature of 123 and slow cooled it to 980°C. A cooling rates of 1°C/hr, gave a good grain aligned microstructure with a small amount of fine sized 211 inclusions. The J_c obtained was about 10^5 amp/cnr at 77 K in zero field.
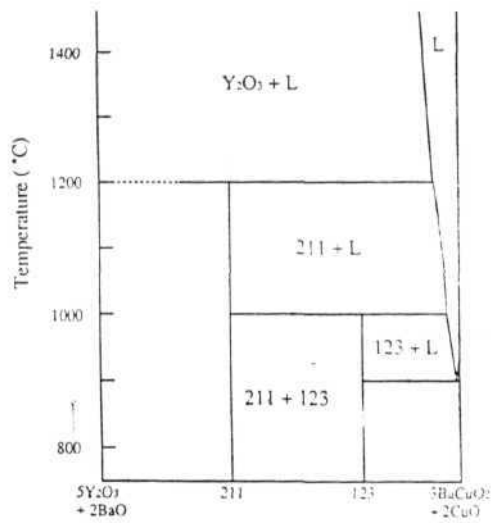
Fig. 1.2 : Psuedo-binary phase diagram of 123.

Murakami *et al.* [11] started with a new process of melt growth, called the Quenched melt growth process (QMG). The 123 sample is kept above the peritectic decomposition of the 211 phase i.e above 1200°C for a small period and then it is quenched to room temperature. The sample has Y_2O_3 + solidified liquid. Again the sample is held above the peritectic decomposition temperature of 123 i.e., above 1010°C for a brief moment where the sample reacts to form 211 + liquid phase, then the sample is slow cooled from T_p to 980°C. Even though the microstructure resembles that of samples melt processed by other variants of the technique, the essential difference is that the 211 particles are distributed uniformly having a much smaller size. The presence of the 211 particles in the microstructure will be beneficial for improvement of J_c, where the non-superconducting contribute to the creation of flux pinning centers. Hence an excess of 211 phase was taken in the starting material so as to retain a large fraction of 211 particles after the **melt** growth. The J_c was reported to have increased by such an addition. By this process there was an agglomeration of the Y_2O_3 particles, to reduce it the process **was** modified to evolve the melt powder melt growth. This is similar to the QMG process but after the high temperature quenching the sample was ground and pressed into pellets, subsequently the usual melt growth schedule was followed. By this the 211 particles were refined to 2-5 urn.

In all variants of the process, the essential step is melting the 123 phase at the 211 + liquid phase region and slow cooling the sample from $T_\sim$ to some lower temperature. If the sample is not held above T_p, the sample will develop pores and if the sample is held for a long time, the 211 particles will coarsen. Thus the

sample should be kept at a suitable temperature above T_p for an optimum period of time **for the** uniform melting of 123 phase and **nucleation of** 211 particles. **The** cooling rates through T_p should be low for stable solidification leading to a better microstructure and properties. 1"C/hr is an optimum cooling rate. The unreacted 211 particles are due to the slow kinetics of the peritectic reaction or shift in **the** liquid phase stoichiometry due to possible reactions with the substrate. Another factor is that, the growth rate of 123 is not perfectly coincident with the dissolution rate of the 211 phase.

The melt processing techniques can be divided into four categories, namely (A) Non-Directional melt texturing, (B) Directional melt texturing, (C) Seeding, & (D) Oxygen controlled melt growth.

1.1.1. Non-Directional Melt Texturing: If the sample while **melt** growth, is slow cooled without an imposed temperature gradient then it is called as non-directional melt growth. The resulting sample consists of multiple domains, which are randomly directed with respect to one another. The boundaries separating these domains are high-angle boundaries, which may contain non-superconducting phases. The reason for the large number of boundaries is because, the conditions are favorable for nucleation of multiple 123 nuclei, although the cooling is carried out maintained at a slow rate to minimize the degree of undercooling. The above mentioned process of Jin *et al.* [9], Salama *el al.* [10] and Murakami *el al.* [11] are mostly non-directional methods. Eventhough the J_c is high **within** the domains, across them the J_c drops down to a low value in non-optimally processed samples.

1.1.2. **Directional Methods:** Directional solidification has the potential of producing textured superconductors that are aligned over long lengths. This difference occurs because the specific location where solidification proceeds can be controlled and multiple nucleation of 123 can be avoided. The directional method involves the relative motion between hot zone and sample, which can be achieved by the movement of either the sample or furnace. In addition, a longitudinal temperature gradient is provided in the hot zone in order to provide directionality to the growth process. McGinn *el al.* [12], Meng *el al.* [13], have used this method to process the samples. Selvamanickam *et al.* [14], have modified the process to provide a high longitudinal-to-lateral temperature gradient to orient the ab-plane close to the sample axis. This was done by putting two heaters, one is kept above the peritectic temperature and another at a temperature corresponding to the nucleation temperature. The microstructure consists of the ab-planes aligned parallel to the sample length and the resulting samples were reported to have a high J_c. But large sized samples cannot be processed by the directional method because of the design considerations.

1.1.3. Seeding: Certain materials like powders of Sm_2O_3, Nd_2O_3, and single crystal MgO can be used as nucleation centers for 123 [15]. When a small amount of these materials are placed on top of a 123 sample, which is then subjected to a non-directional melt texturing, grain growth of 123 around the nucleation centers is enhanced. Since the melting points of these materials are higher than the peritectic temperature of 123, they can act as heterogeneous nucleation centers during the slow cooling phase of melt texturing. The 123 single domain underneath these nucleation centers is found to resemble the geometry of the centers. However, the

crystal orientation of the growth does not follow that of the nucleation source. In contrast, single-crystal or melt textured quasi single crystal Sm-123 has been shown to be an effective seed for the Y-123 superconductor [16]. The seed is defined as a nucleation center where the orientation of growth is controlled by crystal structure of the nucleation source. Because of the higher melting temperature of Sm-123, the seed remains in a solid form, when the Y-123 is heated past its pcritectic temperature. On slow cooling, epitaxial growth of Y-123 occurs at the Sm-123 - liquid +Y-211 interface due to the similar lattice parameters of the two 123 compounds. With the epitaxial growth of 123, the crystal orientation of the superconductor can be customized to fit the geometry of the sample through selective cutting of the seed. The microstructure of the samples show aligned ab-planes in a favorable direction and the samples have high J_c

1.1.4. Oxygen Controlled Melt Growth:

In the RE-123 system, apart from Y-123 other rare earth compounds also become superconducting. However, melt texturing in air/oxygen cannot be applied to them because of the large ionic radii (Nd, Sm) of the rare earth atoms, they form a solid-solution formation of the type $RE_{1-x} Ba_{2-x} Cu_3 O_y$. The rare earth gets substituted at the Barium site leading to off-stoichiometric compounds with low-T_c and J_c. It is reported that by processing in oxygen poor atmosphere (OCMG process) Nd-123 and Sm-123 have been solidified giving T_cs above 90 K and high J_c even in high fields [17,18]. The low oxygen partial pressure suppresses the solid-solution formation to a large extent.

1.2. ADDITIONS IN MELT TEXTURED SAMPLES

Various additions like insulating 211, Pt, CeO_2, ZrO_2, $BaSnO_3$ etc. [19-26], have shown improvement in the microstructure and the J_c. 211 particles are left back in the melt textured samples because of the kinetics of the reaction and liquid phase loss. The presence of it on the 123 matrix is important from the point of flux pinning. If excess 211 phase is taken in the starting material, more of it can be trapped in the matrix. Thus contributing to an increase in flux pinning and J_c. Murakami *el al.* [19] have observed an increase in J_c for 211 additions. Jin *et al.* [20], observed no change, where as McGinn *et al.* [21] observed decrease in J_c for increasing 211 concentrations. Lee *et al.* [22] have explained that for low additions the J_c increases and then it remains constant, but for high additions the J_c decreases with 211 content. The source of the increase in flux pinning is from the **crystallographic** defects around **the** 123/211 interface. Other additions like Ag, Pt, CeO_2 etc. [23-36], have been used to refine the trapped 211 particles at the peritectic melting stage so as **to** result in finer sized 211s after melt processing. These fine sized 211s contribute for an enhancement of J_c, because of the defects present around them.

1.3. MICROSTRUCTURE

The microstructure of melt processed samples largely depends on the process, starting material and additions if any. Samples processed by the non-directional melt texturing have multiple domains of different sizes, because of the

multiple nucleation of 123 [27]. Samples processed by directional melt texturing have limited number of domains and the ab-planes can be aligned along a preferred direction parallel to the sample axis. Each domain consists of parallel plates of 123 grains aligned along a common direction. The parallel platelets are separated by narrow gaps containing liquid phases or other impurities. The secondary phases between the domain boundaries can be reduced by taking excess 211 phase in the starting material, because it ensures complete reaction of liquid phases. The size of the 211 particles trapped in the matrix depends on the process, starting material and additions. In the MPMG process [11], the average particle size is smaller in comparison to other processes [9,10], and it is of the order of 3-5 μm. The microstructural features like the platelet width, gap width, porosity and the average size of 211 particles decreases with increase in the added 211 concentration in the starting material. A concentration of 30 mol % of Y-211 in Y-123 was found to be optimum for obtaining a microstructure which supports high J_c [19]. Additions like Pt, CeO_2 etc. [23-26], refine the particle size to ~1 urn, which contributed to an enhanced J_c. The high J_c is because of increase in flux pinning from the crystallographic defects, which were identified using TEM measurements.

TEM studies show that the melt textured samples contain many defects like twins, stacking faults, and dislocations [28,29]. Twins occur when the structure of 123 changes from tetragonal to orthorhombic during oxygenation. The stresses created during this transformation are released by the formation of twins. The twins are observable both by polarized light optical and transmission electron microscopy. The twins observed by optical microscopy are domains, in which micro-twins are present as substructure. Twins that are not observable by optical

microscopy in the samples with 211 inclusions, the presence of it in can be confirmed by TEM. As the 211 concentration is increased, the size of the **twin** domain becomes small, but there will be no difference in twin structures. The twins play an active role in flux pinning and thus contribute for enhancement of J_c. Besides twins, stacking faults are also seen at higher magnification using TEM. A stacking **fault** has a structure with an extra CuO plane inserted to the chain site of Y-123. These faults enhance flux pinning, but it is very difficult to tailor make a material with the required number of defects. Minimization of these extended defects is a prime requisite for obtaining high J_c s in the melt textured materials.

1.4. FLUX PINNING & CURRENT DENSITY

Melt processed samples have high J_c than sintered samples because of the aligned microstructure, presence of flux pinning sites and absence of high **angle** grain boundaries in the direction of current path. The J_cs are of the order of 10' amp/cm, at 77 K in self fields **[33].** The J_c is less sensitive to applied field if it is along the c-axis orientation of the sample, in comparison to the case when **the** applied field is perpendicular to it. This indicates that J_c-H behaviour is anisotropic. because the pinning is higher when the current is flowing in the basal plane than across it [33].

Significant progress has been **achieved** in increasing the pinning **sites** through process variations. The factors **that** can influence flux pinning in a superconductor include the size, spacing and superconducting properties of **the**

pinning centers, as well as the rigidity of the flux line lattice [34]. In particular, the dimension of the pinning sites is an important parameter in determination of the pinning force in the superconductor. Generally, a pinning center is most **effective if** its dimension is approximately equal to the coherence length (ξ). Crystallographic defects like twin planes, stacking faults and dislocations are effective pinning centers [35]. Non-superconducting particles can also act as pinning centers as the interface acts as a pinning center. For a sharp interface the pinning will be higher as the change in the energy will be higher. Presence of a superconductor with a lower T_c than the bulk T_c of the material is very effective in increasing J_c in high fields, because the low-T_c phase turns normal and acts as pinning center. Due to the presence **of** low-T_c regions, Y-123 melt textured and single crystal samples exhibit a peak in the M-H loop below T_c and in high fields [36]. The low T_c regions are oxygen ordered ortho-II regions [37], which have a $T_c \sim$ 60 to 90 K. These regions are formed due to a spinodal decomposition when the sample is slow cooled during **oxygenation** process [38]. The low-T_c regions will be distributed on a nanometer scale and **will** be effective at high temperatures and fields, as they turn normal and act as pinning centers resulting in a second peak in the M-H loop.

Samples **of** melt textured LRE-123 (LRE= Nd, Sm,..) and single **crystal** also exhibit the peak effect in the M-H loop. Murakami *et al*. [39] have offered an explanation for this effect, due to the pinning from low-T_c regions formed due **to** the solid-solution regions, where the rare-earth substitutes at the Ba-site. **Nakamura** *et al* [40] have shown in TEM images that a dilute concentration of a second phase in the microstructure is responsible for the peak effect. The second phase was concluded to be the low-T_c LRE substituted Ba regions. The proof about the exact

structure of the second phase does not exist. This concept has to be explored to identify the source of pinning in LRE-123 melt textured samples for the peak effect.

A possible mechanism by which the J_c can be improved is by irradiating the melt textured samples with different high energy beams. By irradiation of the samples, fine scale defects of a few nanometers is artificially introduced into the matrix. The defect structure is, small regions of vacancies created during irradiation, which combine into defect clusters. These defects have a different (lower) superconducting order parameter with a characteristic spatial extent [41] j, and are effective as flux-pining centers due to their small dimensions.

1.5. IRREVERSIBILITY LINE

Muller el al. [42] observed that the field-cooled and zero-field cooled magnetization curves as a function of temperature merged into a common reversible behavior. Studying this merging-point as a function of the applied field H, they found that the temperature shifted with field as

Where, T* is a temperature lower than the bulk T_c of the sample and the power q is close to 2/3.

Such an effect is similar to magnetic spin glasses. Muller et al. [42,43] called this a "quasi-de-Almeida-Thouless" line. As the spin-glass derivation is not relevant to the superconducting case, this line is termed as 'irreversibility line' (IR

line) [44]. However, there exists a difference between the dc irreversibility line and the IR line determined from ac susceptibility & resistivity measurements. The irreversibility line (IR line) in the H-T plane divides the region below which the properties are reversible and above are irreversible. It is also a indication of the pinning strength in the sample. For higher pinning strength the line will be steeper, indicating that higher fields are needed to drive the sample to irreversible region, at a particular temperature. The Y-Ba-Cu-0 system has a steeper IR **line, in** comparison to Bi-, or T1-, systems [45]. Hence it is an ideal material for developing as components for practical applications. The melt textured materials of Y-123 system have a higher IR line in comparison to the sintered samples, indicating that by melt texturing **the** pinning strength has increased which results in higher J_cs [46]. The IR line of melt textured samples is found to be higher for samples with increased 211 concentration (30 mol %), indicating that the J_c has increased because of higher pinning strength.

1.6. MAGNETIC RELAXATION

Magnetic relaxation is a phenomenon in which the magnetic moment deacys with time in a logarithmic manner. Large relaxation was observed in all the known families of high temperature superconducting materials. Magnetic relaxation was first studied in low temperature superconductors, but the effect was small. Anderson and Kim [47] introduced the concept of thermal activation of magnetic flux lines out of pinning sites, which proceeds at **a** rate proportional to cxp(-U/kT), where U represents the activation energy and kT the thermal energy.

This leads to a logarithmic decay of magnetic moment with time. This model failed to explain some important details of the magnetic relaxation effect in high temperature superconductors. Careful studies over many orders of magnitude in **time** revealed deviations from logarithmic decay of moment. These led to development of new phenomenological models based on Beasley *et al.* [48] to consider complex current dependent activation energies. The basis of the model involves the collective interaction of flux lines, and hence it is referred to a "collective flux creep". The theory has explained some important aspects of the experimental data. Magnetic relaxation at ultra low temperatures is unexpected on the basis of thermal activation of flux lines. However, temperature-independent relaxation was measured at millikelvin temperatures [49], which led to the novel concept of relaxation based on a quantum tunneling of vortices [50].

     Thermal activated flux motion also causes the broadening of the magneto-resistive curves [51], and determines the shape of the voltage-current (V-I) or electric-field / current density (E-J) curves, causing them to show a power law behavior [52]. Its origin lies in the fact that flux motion is associated with a Lorentz force, which drives the flux lines out of the pinning Sites, and with an electric field $E = (1/c) B \times v$, where v is the average velocity of the flux lines in the direction of the Lorentz force. For an unpinned damped flux-line lattice, v is proportional to the current density (J), and obtains a linear relationship between V and I [53]. When pinning is important the average velocity is $v = v_o \exp[-U(J)/kT]$, where the prefactor v_o may also be a function of J. So E is also exponentially dependent on U(J). Thus relaxation is associated with a highly non-linear V-I

16

relationship, dictated by the specific dependence of U on J and by the exponential dependence of E on U.

Relaxation manifests in many other ways. It causes the irreversible part of the magnetic torque to be time dependent [54], and influences the ac magnetic response [55], its harmonics [56], and its frequency dependence [57]. It couples to acoustic and optical signals [58] and causes electrical and magnetic noise [59]. Magnetic relaxation in high-temperature superconductors is important for several reasons. From a fundamental perspective, it has led to the theoretical understanding and elaboration of cooperative theory of thermal activation and development of the novel concept of quantum creep. This understanding has also contributed to the broader view of the magnetic phase diagram and pinning mechanisms and on improved determination of the thermodynamic properties of high temperature superconductors. From an applied view, the importance of magnetic relaxation lies in the fact that it modifies the current-voltage characteristics of high temperature superconductors, determines the temperature and time dependence of J_c and dictates the limits to the stability of superconducting devices such as persistent-mode magnets. These properties are central to the successful commercialization of high temperature superconductor technology.

1.7. APPLICATIONS

The melt textured samples are being investigated use in various applications. The first application that comes from its diamagnetic property, is levitation platforms. This happens because of large flux pinning in these samples.

Successful fabrication into bearings of melt processed bulk Y-123 has been reported. [60]. The Y-123 sample is used a stator and a permanent magnet for the rotor. The attractive and repulsive forces between them cause the stator to be suspended in mid-air, where it is thus able to spin freely. Superconductor flywheels can be an excellent energy storage devices. Where a magnet is placed on top of a superconductor and is rotated, because of lack of friction, the magnet can rotate for a long time. This concept can also be used in transportation system, where a train can move on rails without friction, touching high speeds. A superconductor magnet is another possibility for these materials. Because of strong flux pinning, field can be trapped inside the material without decaying for a long time. This property can be used to design a magnet to give a required field.

OBJECTIVES

The objectives of this thesis is the following:

(1).   Melt process the Sm-123 system in low oxygen atmospheres using the Solid Liquid Melt Growth route (SLMG) . The low oxygen atmosphere was used to suppress the solid solution formation of the nature $RE_{1-x}Ba_{2-x}Cu_3O_y$. This forms because of the similar ionic radii of the rare earth and Ba atom. In the SLMG route the precursors are taken in the form of 211 + liquid phases, instead of the 123 phase in the conventional melt processing methods.

(2).   The insulating Sm-211 concentration was increased systematically in the starting material from 0 to 40 mol %. Its effect on the microstructure and superconducting properties like the current density, Irreversibility line and flux creep is investigated. In literature no such report exists about the systematic variation of the Sm-211 concentration in melt textured Sm-123, to arrive at an optimum concentration of Sm-211 for obtaining high J_c. The study will offer an explanation for the observed microstructural features and the behaviour of J_c with increasing Sm-211 concentration. The origin of the pinning for the anomalous peak effect in M-H loop will be investigated from TEM studies. The behaviour of the magnetic relaxation for the samples having peak effect is also investigated.

(3).   Additions like Ag, CeO_2, ZrO_2, PrO_2 in small amounts were added to the starting material of Sm-123 sample with 30 mol % Sm-211. This was done with an objective to refine the trapped 211 particles in the microstructure of the melt processed sample. As the refined 211s are supposed to increase the current density

as they enclose large number of crystallographic defects around them. The effect of these additions on the microstructure and the current density is investigated.

(4).   A novel processing technique to process a near-net shaped components free of macro delects with high J_c was developed in Y-, Gd-123 system [61]. **The processing technique known as Infiltration-Growth (1G) process, is done here in Sm-123 with a similar objective to process the samples free of macro defects** The microstructure and behaviour of J_c, 1R line, and relaxation is investigated.

REFERENCES :

1. **J. G. Bednorz** and K. A. Muller, **Z. Phys.** B **64**, 189 (1986).

2. M. K. Wu, J. R. Ashburn, C. J. Torng, P. H. Hor, R. L. Meng, L. Gao, Z. J. Huang. Y. Q. Wang, and C. W. Chu , Phys. Rev. Lett. **58**, 908 (1987).

3. H. Maeda, Y. Tanaka, M. Fukutomi, and T. Asano, Jap. J. Appl. Phys. 27, 1.209 (1988).

4. A. M. Herman, Z. Z. Sheng, D. C. Vier, S. Schultz, and S. B, Oseroff, Phys. Rev. B 37, (1988)9742.

5. S. N. Putillin, E. V. Antipov, O. Chenaissem, and M. Marezio, Nature **362**, 226 (1993).

6. J. E. Greedan, A. H. O'Reilly, and C. V. Stager, Phys. Rev B **35**, (1987) 8770.

7. J. M. Tarascon, W. R. McKinnon. L. H. Greene G. W. Hull, and E. M. Vogel, Phys. Rev. B 36, (1987) 226.

8. D. C. Larbalestier, Physics Today 6, 74 (1991).

9. S. Jin, T. H. Tiefel, R. C. Sherwood, R. V. van Dover, M. E. Davis, G. W. Kammlott, and R. A. Fastnacht, Phys. Rev B 37, (1988) 7850.

10. K. Salama, V. Selvamanickan, L. Gao, and K. Sun, Appl. Phys. Lett. 54. 2352 (1989).

11. M. Murakami, M. Morita, K. Doi, and K. Miyamoto, Jap. J. Appl. Phys. 28, (1989) L1 125.

12. P. McGinn, N. Zhu, W. Chen, S. Sengupta and T. L. Ward and D. M. Kroeger, Appl. Phys. lett. **57,** 1455 (1990).

13. R. L. Meng, C. Kinalidis, Y. Y. Sun, L. Gao, Y. K. tao, P. H. Hor, and C. W. Chu, Nature **345, (1990)326**.

14. V. Selvamanickam, C. Partsinevelos, A. V. McGuire, and K. Salama, Appl. Phys. Lett **60,** (1990)3313.

15. M. Murakami, Bulk Materials (*Processing & Properties of High-T$_c$ Superconductors*) 1993.

16. M. Morita, S. taebayashi, M. Tanaka, K. Kimura, K. Miyamoto, and K. Sawano, Adv. Supercond. 3, (1991) 733.

17. S. 1. Yoo, M. Murakami, T. Higuchi, N. Sakai, J. Weltz, N. Koshizuka and S. Tanaka, Japn. J. Appl. Phys. **33, (1994) L715**.

18. M. Murakami, S. 1. Yoo, T. Higuchi, N. Sakai, J. Weltz, N. Koshizuka and S. Tanaka, Japn. J. Appl. Phys. **33,** (1994) L1000.

19. M. Murakami, H. Fujimoto, S. Gotoh, K. Yamaguchi, N. Koshizuka. and S. Tanaka, Phvsica C **185-189, (1991)321**.

20. S. Jin, T. 11. Teifel, and, G. W. Kammlott, Appl. Phys. Lett 59, (1991) 540.

21. P. McGinn, N. Zhu, W. Chen, S. Sengupta, and T. Li, Physica C **176**, (1991) 203.

22. D. F. Lee, V. Selvamanickam, and K. Salama, Physica C **202,** (1991) 83.

23. N. Ogawa, I. Hirabayashi and S. Tanaka, Physica C **177,** (1991) 101.

24. C. J. Kim, S. L. Lai, and P. J. McGinn, Mater. Lett. 19, (1994) 185.

25. T. Oka, Y. Itoh, Y. Yanagi, H. Tanaka, S. Takashima, Y. Yamada, and U. Mizutani, Physica C **200,** (1992) 55.

26. P. J. McGinn, W. Chen, N. Zhu, C. Varanasi, L. Tan, and D. Balkin, Physica C **183,** (1991) 51.

27. K. Salama and D. F. Lee, Sup. Sci. & Tech. 7, (1994) 177.

28. M. Mironova, D. F. Lee and K. Salama, Physica C **211,** (1993) 188.

29. Z. L. Wang, A. Goyal, and D. M. Kroeger, Phys. Rev. B 47, (1993) 5373.

30. S. Nakahara, S. Jin, R. C. Sherwood, and T. H. Tiefel, Appl. Phys. Lett 54, (1989) 1926.

31. K. Yamaguchi, M. Murakami, H. Fujimoto, S. Gotoh, N. Koshizuka, and S. Tanaka, Jap. J. Appl. phys. 29, (1990) L1428.

32. M. Daumeling, J. M. Seuntjens, and D. C. Larbalestier Nature **346,** (1990) 332.

33. J. W. Ekin, K. Salama, and V. selvamaickam, Nature **350,** (1991) 26.

34. D. Dew-Hughes , Philos. Mag **30,** 293 (1974).

35. K. Yamaguchi, M. Murakami, H. Fujimoto, S. Gotoh, T. Oyama, Y. Shiohara, N. Koshizuka, and S. Tanaka, J. Mater. Res. 6, (1991) 1404.

36. M. Daumeling, J. M. Seuntjens and D. C. Larbalestier, Nature **346,** (1990) 332.

37. R. Beyers, B. T. Ahn. V. Y. Lee. S. S. P. Parkin, M. L. Ramirez, K. P. Roche, Vazques, T. M. Gar and R. A. Higgins, Nature **340,** (1989) 619.

38. S. Semenovskaya and A. G. Khatchaturyan Physica D 66, (1993) 205.

39. T. **Egi,** J. G. Wen, K. Kuroda, H. Unoki and N. Koshizuka, Appl. **Phys. Lett,** 67, (1995)2406. ,

40. M. Nakamura, **T. Hirayama, Y.** Yamada, Y. Ikuhara and Y. Shiohara. **Japn.** J. **Appl. Phys. 35,** (1996) 3882.

41. R. B. Van-Dover, E. M. Gyorgy, A. E. White, L. F. Schneemeyer, R. J. **Felder,** and J. V. Waszczak, Appl. Phys. Lett 56, (1990) 2681.

42. K. A. Muller, M. Takashinge & J. G. Bednorz, Phys. Rev. Lett. 58, (1987) 908.

43. 1. Morgenstern, K. A. Muller & J. G. Bednorz, Z. Phys. B 69, (1987) **33.**

44. D. M. Ginzberg, *Intoduction to Superconductivity.*

45. Y. Yeshurun, A. P. Malozemoff, T. K. Worthington, R. M. Yandrofski, L. Krusin-Elbaum, F. Holtzberg, T. R. Dinger & G. V. Chandrashekar, Int. Conf. On Ctrical Currents in High Temperature Superconductors, August 16-19, 1988, Colorado, USA.

46. M. Muralkami, S. Gotoh, N. Koshizuka, S. Tanaka, T. Matsushita, S. Kambe, and K. Kitazawa, Cryogenics 30, (1990) 390.

47. P. W. Anderson, Phys. Rev. Lett. 9, (1962) 309.

   P. W. Anderson and Y. B. Kim, Rev. Mod. Phys. 36, (1964) 39.

48. R. M. Beasley, R. Labusch, and W. W. Webb, Phys. Rev. **181,** (1969) 682.

49. A. C. Mota, Pollini, K. A. Visani, K. A. Muller and J. G. Bednorz, Phys. Scr. 37,(1988)823.

50. G. Blatter, M. V. Feigel'man, V. B. Geshkenbein, A. I. Larkin, and V. M. Vinokur, Rev. Mod. Phys. 66, (1994) 1125.

51. J. M. Graybeal and M. R. Beasley, Phys. Rev. Lett. 56, (1986) 173.

52. R. H. Koch, V. Foglietti, W. G. Gallagher, G. Koren, A. Gupta and M. P. A. Fisher, Phys. Lett. 63, (1989) 1511.

53. J. Bardeen and M. J. Stephen, Phys. Rev. 140, (1965) A1197.

54. C. Giovannella, G. Collin, P. Rouault and I. A. Campbell, Europhys. Lett. 4, (1987) 109.

55. M. Nikolo and R. B. Goldfarb, Phys. Rev. B 39, (1989) 6615.

56. A. Shaulov and D. Dorman, Appl. Phys. Lett. 53, (1988) 2680.

57. A. P. Malozemoff, T. K. Worthington, Y. Yeshurun, F. Holtzberg, and P. H. Kes, Phys. Rev. B 38, (1988) 7203.

58. E. Zeldov, N. M. Amer, G. Koren, A. Gupta, R. J. Gambino, and M. W. McElfresh, Phys. Rev. Lett. 62, (1989) 3093.

59. J. R. Clem, Phys. Rep. 75, (1981) 1.

60. F. C. Moon, Appl. Phys. Lett 56, (1990) 397.

61. E. Sudhakar Reddy and T. Rajasekharan, J. Mater. Res, (In Press).

CHAPTER II

<u>EXPERIMENTAL</u>

2.1. MELT GROWTH PROCESS

In melt texturing, the samples are melted above the peritectic temperature of the system and then slow cooled. The first step involves preparing the precursor powders and secondly subjected to the melt processing schedule. Firstly the powder preparation is described and then the melt processing.

(a). POWDER PREPARATION

The precursors were taken in the form of $Sm-211$ + liquid phases, as the SLMG route [1] was followed. The liquid phases comprises of BaCuO, and CuO. $Sm-211$ and $BaCuO_2$ were prepared by solid-state sintering route. This consists of taking the constituent compounds in the form of oxides or carbonates, according to the **stoichiometry** and mixing thoroughly using an organic solvent as a medium. The mixtures will be dried and calcined at a temperature corresponding to the phase formation. Usually two calcinations are done for phase purity. For the Sm-211 and $BaCuO_2$ powder preparation; required amounts of Sm_2O_3, $BaCO_3$ and CuO were taken according to stoichiometry and mixed in a centrifuge mill. The mixtures were taken in an agate pot having agate balls for uniform mixing. The organic used was Acetone, the mixing was done for two hours. Then the mixture was dried in oven for 12 hours, later it was calcined at 975°C for $Sm-211$ and $900°C$ for BaCuO,

respectively. The calcination was repeated twice with an intermediate grinding **for** phase purity.

For melt processing required amounts of Sm-211, $BaCuO_2$ & CuO were taken according to the composition of the sample. The precursor powder was mixed thoroughly in a mortar & pestle using Acetone as a medium. The powder was dried and pressed **into** a pellet under a uniaxial press. Samples **of the** dimension 15mm x 15mm x 10mm were subjected to melt processing. For the Sm-211 & other additions, the precursors were taken according to the requirement before grinding the constituents.

(b).   MELT GROWTH SCHEDULE

The samples were processed in commercial Argon atmosphere, which has an oxygen content of 4 ppm. A tubular furnace having an Alumina muffle with A-1 **Kanthal** elements wound on it was used for melt processing. Accurate temperature control was achieved by using a programmable PID controller. The two outer ends of the furnace were sealed with Syndiana caps to prevent entry of atmosphere gases into it. Temperature gradient was present on the sample as there was no measurable gradient in the region where the sample was kept in the furnace. Melt processing was done by a schedule as given in Fig. 2.1, i.e., by melting the sample at $1115^{\circ}C$ for 10 minutes and then slow cooling from $1060^{\circ}C$ to $950^{\circ}C$ at a rate of $1^{\circ}C/hr$. Oxygenation of the samples was done by cooling the samples in flowing oxygen atmosphere from 600"C to 250"C according to the schedule :

$$\begin{array}{ccccc} & 6hrs & 12hrs & 24hrs & 48hrs \\ 600^{\circ}C & \rightarrow 500^{\circ}C & \rightarrow 450^{\circ}C & \rightarrow 350^{\circ}C & \rightarrow 250^{\circ}C. \end{array}$$
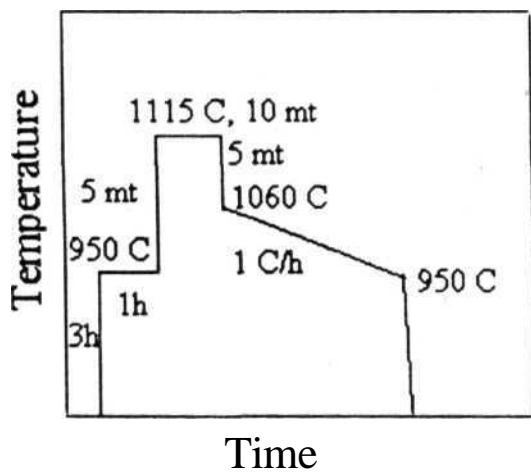
Fig. 2.1 : Melt processing schedule of for the preparation of the Sm-123 samples.

2.2. CHARACTERISATION

2.2.1. X-RAY DIFFRACTION

X-ray diffraction patterns of the melt processed samples were recorded using Philips X-ray diffractometer. The pattern was recorded from 20° to 60° with a step of 2°/min. The recorded patterns were indexed for the phases present. The lattice parameters were obtained by a least square refinement of the data.

2.2.2. MICROSTRUCTURAL INVESTIGATIONS

The microstructure of the samples was investigated by optical and scanning electron microscopy. Transmission electron microscopy was done for two samples. The sample preparation is described below.

(a). OPTICAL MICROSCOPY

The optical microscopic investigations was done by preparing the samples following the standard metallographic techniques. The samples were cut into thin slice using an "ISOMET" diamond low speed saw. The sliced samples were mounted for polishing using the cold set mount. Polishing of the samples was done initially on SiC abrasive paper with gradual reduction of the grating paper from 500 to 1000. Final polishing was done on a disk polishing machine having polishing cloth with diamond paste. The grade of the paste was reduced from 10 urn to 0.25 urn for obtaining optically reflecting surface. The polished sample were cleaned with methanol and optical microscopy was done using a microscope fitted

with a polariser. Optical micrographs were recorded with different exposure times depending on the requirement.

(b). SCANNING ELECTRON MICROSCOPY

The sample preparation was essentially the same as described above. The same sample used in optical microscopy was used for SEM investigations. Carbon or Gold coating was not used as the surface was conducting. Both back scattered or / and secondary electron images were recorded, depending on the sample and the area of interest.

(c). TRANSMISSION ELECTRON MICROSCOPY

The sample preparation for TEM investigations was done according to the procedure followed commonly for the superconducting samples. Samples of 3mm disks were cut using an ultrasonic driller. The disks were dimpled with a dimple grinder (Gatan) upto a thickness of 20 μm. Then the sample was further thinned in a Argon-ion mill (Gatan). The beam voltage used was 4 kv with a current of 1.5 mA, at an angle of 20°. Finally the angle was reduced to 11° and milling was continued for 2 hours to allow the sample to be perforated with electron transparent regions at the edge of the perforation. The sample was mounted for TEM investigations. The microscope was operated to form images by bright field, dark field images and to form small area diffraction (SAD) patterns. Using the camera constant method the diffraction patterns were indexed, for identification of the phase present. The accelerating voltage used in the TEM was 160 kv, which is below the value which would irradiate the sample.

2.3.   SUPERCONDUCTING PROPERTIES

The properties studied are the superconducting transition temperature (T_c), current density (J_c), and flux creep in the samples. The T_c was estimated by the four-probe d.c electrical resistivity and SQUID magnetometer. The J_c was estimated by SQUID and VSM measurements. The experimental details are given below.

(a). RESISTIVITY MEASUREMENTS

Standard four-probe d.c electrical resistivity measurements were done on the samples. Electrical contacts were made using silver paint. Two outer contacts were made for passing current in the sample and two inner contacts for measuring the voltage developed in the sample. The temperature was varied by attaching a heater to the sample holder. The sample holder was kept above liquid nitrogen inside a glass dewar. The measurements were done both while cooling and heating, from room temperature to 77 K. For each reading the direction of current was reversed to remove errors in the measurements.

(b). MAGNETISATION MEASUREMENTS

Magnetisation measurements were done on the samples using a Quantum design SQUID magnetometer (Quantum Design). The samples were cut from a single domain with dimensions ~1mm x 1mmx 0.5mm. The field was applied parallel and perpendicular directions to c-axis. The d.c hysteresis loops were recorded by sweeping the field to complete the loop, at a particular temperature.

The loops were recorded at different temperatures on similarly. The J_c of the samples were estimated from the loops using Bean's model.

The J_c is given by the relation.

$$J_c = 20 \, \Delta M/a(1\text{-}a/3b)$$

where AM is the loop width at a particular applied field, a & b are the sample dimensions in centimetres. From the J_c the pinning force is calculated using the relation $F_p \bullet J_c$ B.

Magnetic relaxation measurements were measured using a VSM with the field applied parallel to c-axis orientation of the sample. The measurements are made with a constant field sweep of 100 G/s, resulting in an electric field value of 10^{-2} to 10^{-1} at the sample surface. The irreversibility lines were measured with a J_c criteria of $100 \, A/cm^2$ and the relaxation rate was obtained from measuring M(H) with different dB/dt values. From the data the normalized relaxation rate was estimated from the relation $S = (1/M)(dM/dlnt)$.

REFERENCE :

1. D. Shi, S. Sengupta, J. S. Lou, C. Varanasi and P. J. McGinn, Physica C **213,** (1993) 179.

CHAPTER III

Sm-211 ADDITION

Melt textured $REBa_2Cu_3O_y$ (RE-123) **has** high current density (J_c) because of the superior microstructure and increase in the flux pinning. The microstructure contains features like 123 grains aligned in the ab-plane with reduced number of weak links in the direction of current flow, and with RE_2BaCuO_5 (RE-211) particles distributed in the 123 grains [1]. The presence of 211 particles is **due** to **liquid** phase loss, anisotropic growth rate of 123, and because the rate of dissolution of 211 in the liquid phase is not in accordance with growth rate of 123 [2]. The increase in flux pinning is due to pinning, at the crystallographic defects around the 123/211 interface. Such defects include twins, stacking faults and dislocations [3]. If excess 211 is taken in the starting material, a large amount of it will be left back after the peritectic reaction, which would contribute to increase in flux pinning. Murakami *et al.* *[A]* have observed an increase in J_c, for excess amount of Y-211 in the starting material of melt processed Y-123. McGinn *et al.* [5] observed a drop, and Jin *et al.* [6] reported to have seen no change in J_c, with increase in Y-211 concentration in Y-123 system. Lee *et al.* [7], gave a generalized explanation for the behaviour of J_c with increasing concentrations of Y-211 phase in melt processed Y-123 system. According to them, the J_c increases for low additions of Y-211 phase, and then remains independent of the added Y-211 concentration. For high concentration of Y-211, the J_c drastically drops to a low value, this is because of the reduction in the matrix area. Apart from the flux

pinning property the presence of 211 particles in the microstructure also helps to dissipate mechanical stresses, and thus increases the toughness of the material [8,9].

The microstructural features and the J_c dependence in melt processed Sm-123 system with increasing Sm-211 concentration, is discussed in this chapter. A systematic study on the Sm-123 system in that direction does not exist is not reported. In the literature there exists exhaustive reports about the Y-123 system, with increasing 211 concentration. An increase in J_c for an optimum 211 concentration (30 mol %) has been reported. On similar lines, the dependence of J_c and other related properties is studied with an objective to observe those properties with increasing Sm-211 concentration in melt processed Sm-123 samples. The samples were prepared in reduced oxygen atmosphere and using the Solid Liquid Melt Growth (SLMG) route [10]. The reason for preparing in reduced oxygen atmosphere is to suppress the formation of solid-solution which leads to low-T_c compounds, as discussed in the introduction of this thesis. It is reported that by preparing samples in such a reduced atmosphere the solid-solution formation can be reduced and the resulting compounds will have T_c greater than 90 K [11]. In the SLMG route the precursors used are solid 211 plus liquid phases instead of the 123 phase, and the usual melt texturing schedule is followed. After the peritectic melting, the 211 and the liquid phases are combined to form the 123 phase below the peritectic temperature.

The samples were prepared with increasing concentrations of Sm-211 phase, i.e., from 0 to 40 mol %, in the starting material. Melt processing was done

as discussed in the experimental chapter. The cooling rates adopted while melt texturing were 1"C/hr. The results of these are discussed below.

3.1   PRELIMINARY CHARACTERISATION

The X-ray patterns of all the samples with increasing Sm-211 concentration is shown in Fig. 3.1. These are indexed to the orthorhombic Sm-123 phase, with varying   amounts of Sm-211 [12]. The lattice parameters obtained from the patterns closely matched those reported for the Sm-123 [12]. A decrease in the b and c parameter values, with an increase in the a parameter, characteristic of the low-T_c solid-solution [13] was not noted. Fig. 3.2 shows the dc electrical resistivity measurements of the samples plotted as a function of temperature. The T_c values are above 90 K confirming the minimization of solid-solution formation.

3.2   MICROSTRUCTURAL FEATURES

All the samples had large quasi-single crystalline domains of Sm-123, whose size was observed to decrease, and the number to increase, with the increase in Sm-211 concentration. On an average, the stoichiometric sample had about two domains, the 10 mol % sample had three and the 20, 30, 40 mol % samples had about 9, 15, 25 domains respectively. This happens because, the samples were processed by a non-directional melt growth technique, in which multiple nucleation of Sm-123 takes place. The above observation suggests that an important factor controlling the nucleation of Sm-123 is the concentration of Sm-211 in the starting material.
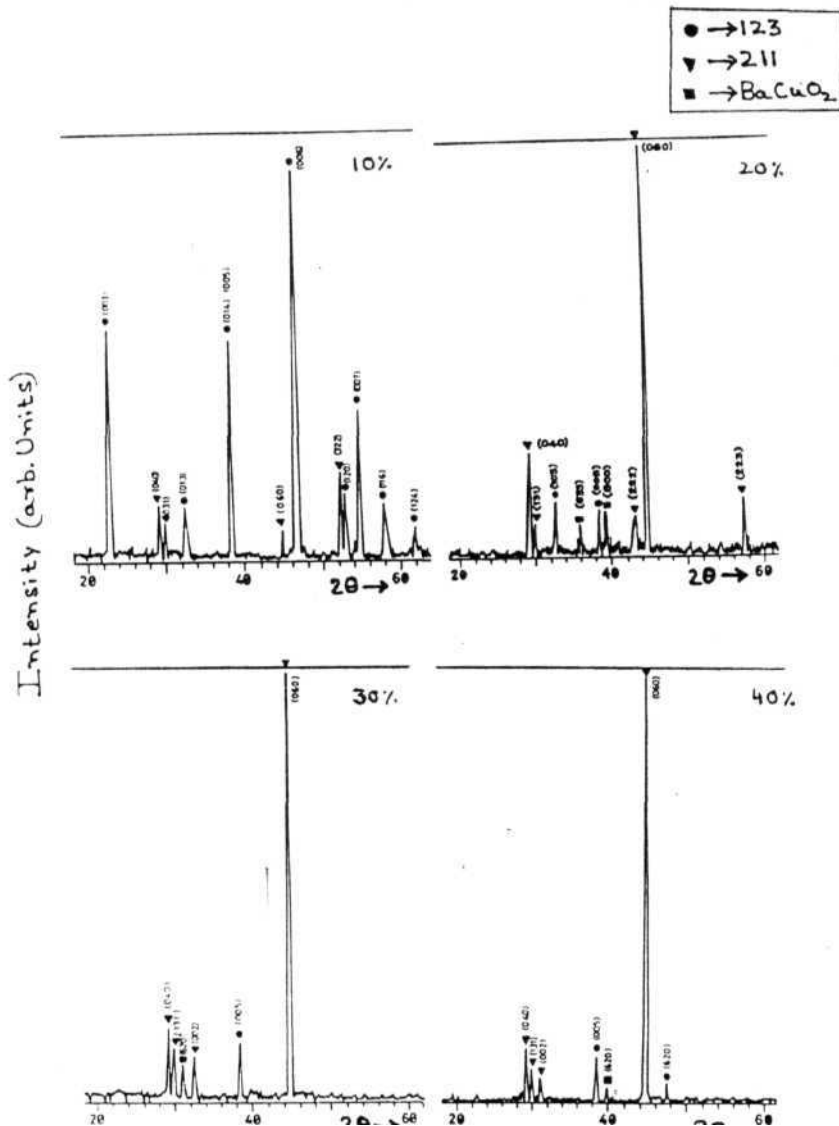
Fig. 3.1 : X-ray diffraction patterns of the samples with Sm-211 concentration of 10, 20, 30 and mol % in the starting material. Peaks corresponding to the solid-solution formation were not observed.
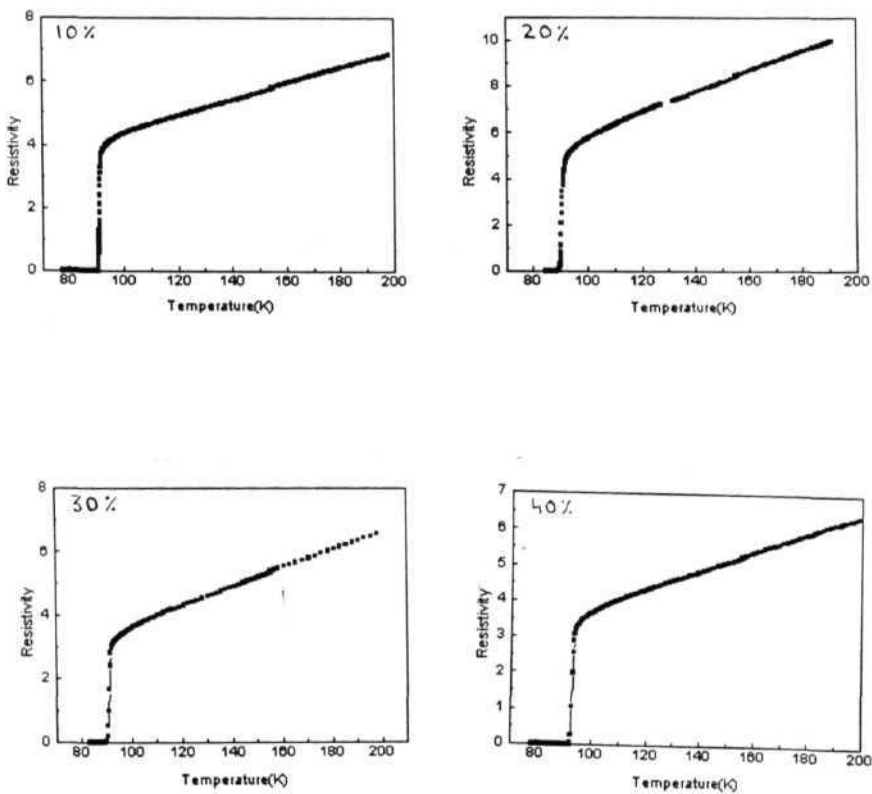
Fig. 3.2 : dc electrical resistivity measurements of the samples as a function of temperature. The T_c of the samples are above 90 K.
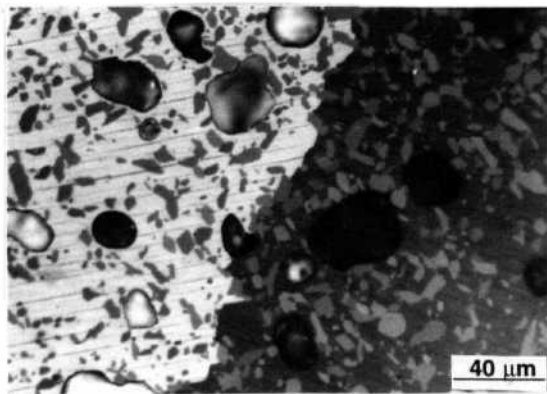
Fig. 3.3 : Representative optical micrograph of the 10 mol % Sm-123 melt processed sample showing two misaligned 123 domains with 211 particles distributed on them.
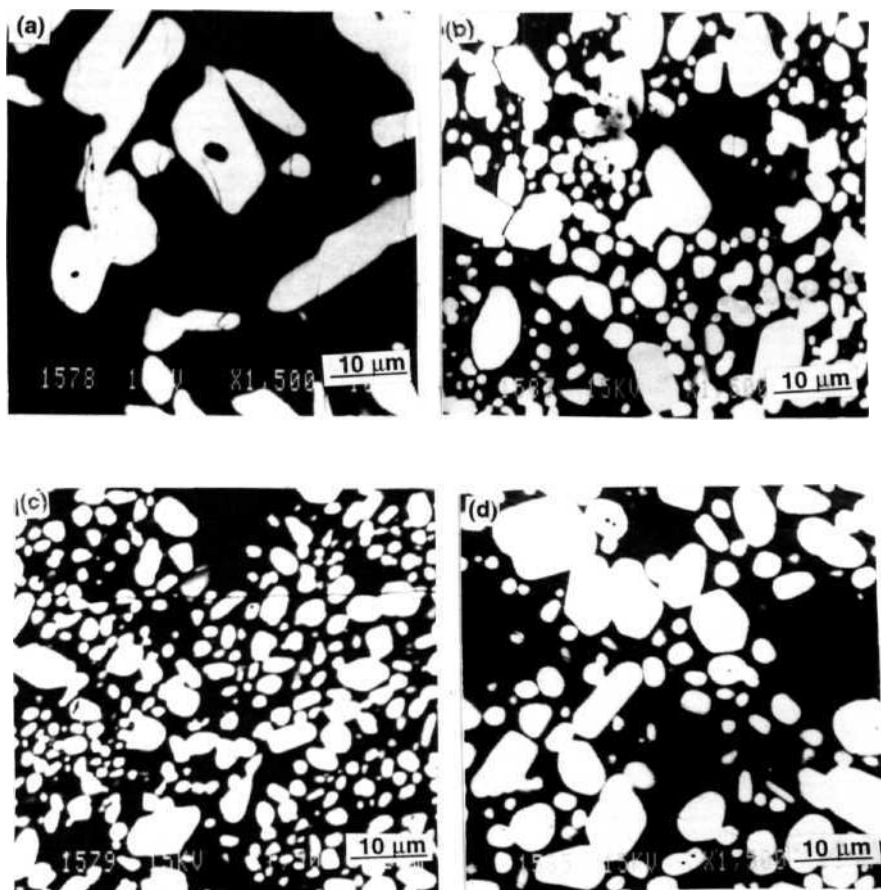
Fig. 3.4 : SEM micrographs of the samples with increasing Sm-211 concentration.

Sm-123 with (a). 10 mol % Sm-211, (b). 20 mol % Sm-211, (c). 30 mol% Sm-211,

(d). 40 mol% Sm-211.

Fig. 3.3 is a representative polarized optical micrograph of the sample. It shows a boundary between two domains aligned in different directions.

The microstructures of the samples (Fig. 3.4) have the usual features observed in melt processed samples [14], namely, parallel platelets of 123 aligned in a preferential direction with 211 particles distributed in them. Some Sm-211 free regions are also seen in the micrographs, and their sizes decrease with increasing 211 concentration. Kim *et al.* [15] have explained the origin of 211-free regions on the basis of oxygen gas evolution during melt processing. Due to a change in the valency of copper during melting, oxygen gas is evolved, and a pore is formed. Since the mobility of liquid phases is more, the pore is likely to be filled by it than by the solid 211 particles. After the peritectic reaction is over, a 211-free region is formed at the pore site. The morphology of the trapped 211 inclusions in the samples change with increasing 211 concentration. In the stoichiometric and the 10 mol % Sm-211 containing sample, the 211 particles have an acicular morphology with a high aspect ratio of ~ 4 to 5. In the 20, 30 and 40 mol % Sm-211 containing samples, the Sm-21 1s have nearly spherical morphology. In Fig. 3.5, a histogram of Sm-211 particle size distribution in the microstructure is plotted, they show a refinement of 211 particles with increasing 211 concentration, except for the 40 mol % sample in which particles are slightly coarsened.

The microstructural features observed above can be explained on the basis of the increasing number of 211 particles in the pro-peritectic liquid with increasing 211 concentration. To explain the microstructural features, the samples after the melting stage (i.e. from 1115°C) were quenched to room temperature and the nature of 211 particles in the peritectic liquid was observed. Fig. 3.6 shows the
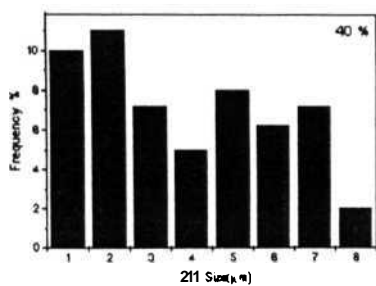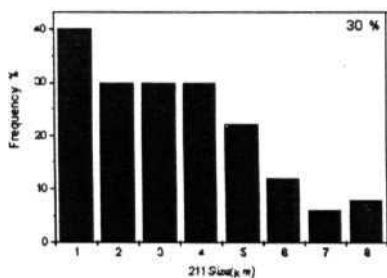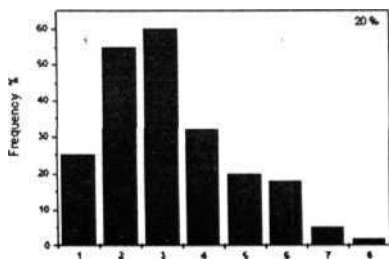
Fig. 3.5 : Histogram plots of the 211 particle size distribution in the micrographs.

(a). 20 mol % Sm-211, (b). 30 mol% Sm-211, (c). 40 mol % Sm-211.
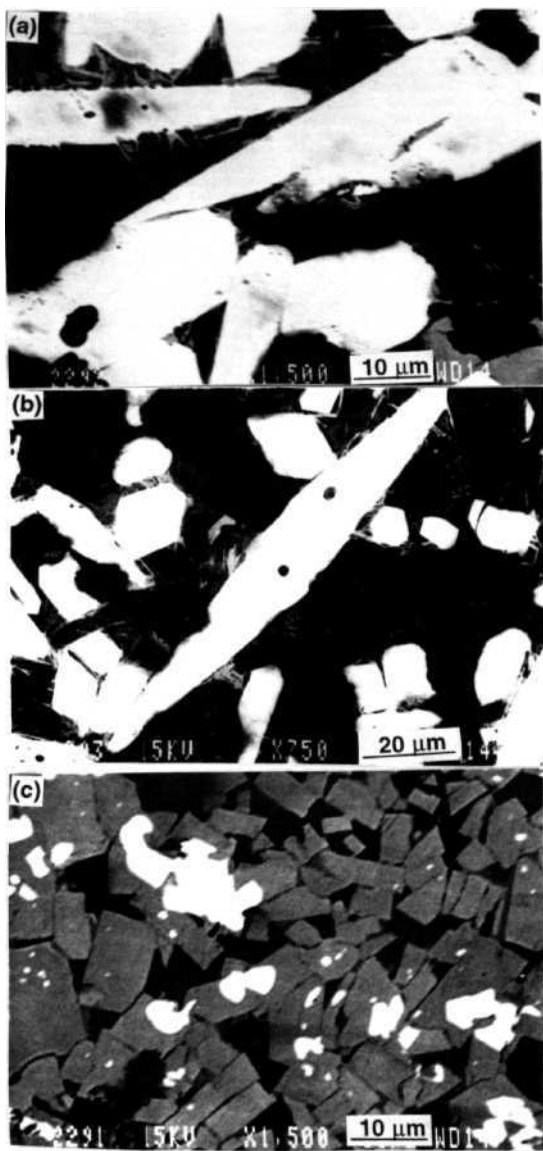
Fig. 3.6 : SEM micrographs of samples quenched form 1115°C to room temperature. (a). Sm-123, Sm-123 with (b). 10 mol % Sm-211, (c). 20 mol % Sm-211.

SEM micrographs of the samples of Sm-123 and Sm-123 containing 10 & 20 mol % Sm-211. It can be seen that the first two samples with lower Sm-211 content have large acicular 211 particles after the melting stage. In the 20 mol % sample, the size of the 211 particles has decreased and they are blocky. The features seen in Fig. 3.6 seem to explain the microstructure of the melt processed samples. The 211 particle size seen in the first two melt processed samples have acicular shape with large aspect ratios because of the shape of 211 particles at the pro-peritectic stage. After the

peritectic reaction, the edges of the 211 particles get rounded off due to its partial dissolution of it during the growth process, but the morphology to a large extent remains same. In the samples with higher concentration of 211 (i.e. 20 to 40 mo! %) a large number of 211 particles occur in the pro-peritectic liquid and they do not have enough space to grow with their natural crystallographic habitat into long rods. In the resulting microstructure the 211 particles appear to be refined. The average particle size of the 211s trapped in the microstructure of the melt textured samples and the nucleated 21 1s at the peritectic melting stage is calculated using standard metallographic techniques [16], and is plotted in Fig. 3.7. The figure shows that with increase in 211 concentration the particle size of it in the microstructure decreases. This is due to the size of the nucleated 211s at the melting stage, for low concentrations it is large and for higher concentrations it is small. In Y-123 system, it has been demonstrated that the smaller sized 211 particles are surrounded by crystallographic defects [17,18]. The defects play an important role in enhancing the J_c as discussed earlier. It remains to be seen in the Sm-123 system whether the J_c is higher when the microstructure contains a large

concentration of small sized Sm-211 particles. However, there is a sudden change above the 10 mol % sample. All the microstructural features change drastically above this concentration. It will be seen below that the magnetic properties also change drastically above the same concentration.

The 211-free regions observed in the microstructures of the melt processed samples can also be explained from Fig. 3.6. The figure shows large areas near the long 211 particles, devoid of 211s. The inhomogeneity in the packing of 211 particles either occurring at the stage of powder consolidation or at the stage of melting due to the development of large acicular 211 particles prevents a packing to 100 % density at the melting stage.
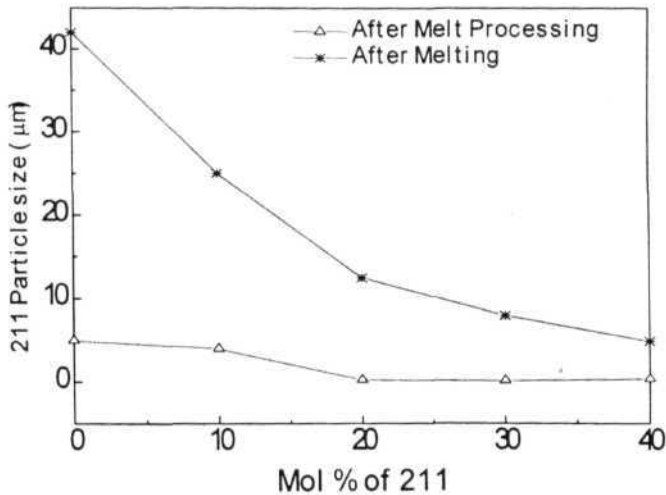
Fig. 3.7. The 211 particle sizes for increasing 211 concentrations, after the high temperature melting and after melt processing.
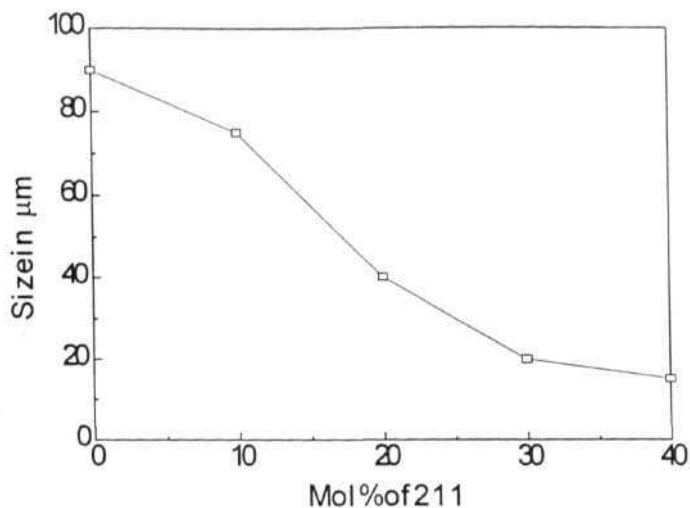
Fig. 3.8 : Plot of 211-free regions observed in the microstructures of samples with increasing 211 concentration.

It has been shown by Sudhakar Reddy *et al*. [19], that almost all the shrinkage during melt processing occurs at the melting stage itself and very little during the subsequent peritectic formation of 123 while cooling. At the peritectic reaction stage below T_p, the inhomogeneous regions in the 2-phase mixture, without 211 get converted to 123 with the absence of 211 inclusions. With increasing 211 concentration, the acicularity of the 211 particles decreases. This can be expected to result in a reduction in size of the 211-free regions with increasing 211 content, as observed in our experiments. The same was observed in Fig. 3.8, which is a plot of 211-free regions with increasing 211 concentrations.

3.3. dc MAGNETIZATION STUDIES

The dc magnetic hysteresis (M-H) loops of the samples processed in low oxygen atmosphere were recorded at 5 K and 77 K for fields applied parallel to the c-axis. The loops are shown in Fig. 3.9. At 5 K, there are no anomalous feature present in the loops. At 77 K for the stoichiometric & 10 mol % sample, have a 'fishtail' or 'peak-effect' at intermediate fields. The effect is more pronounced in the 10 mol % sample. This peak-effect is absent for the rest of the samples at 77 K. The origin of peak-effect was explained by Murakami *et al.* [20] and Egi *et al.* [21], as due to the field-induced pinning from the low-T_c solid-solution regions. Nakamura *et al.* [22], have reported to have observed a tweed morphology within the twin regions of, single crystal Nd-123 sample. It was also mentioned that the features resemble the spinodal decomposition of an aged alloy, with a modulated structure distributed on a nanometer scale. These structures were assumed to be the low-T_c solid-solution regions, which contribute to the field-induced pinning, by turning normal at high fields. It was observed in the Y-123 single crystals, that the microstructure consists of a dilute mixture of ortho-I (T_c = 90 K) & ortho-II (T_c ~ 60 to 90 K) structures generated by spinodal decomposition [23]. Because of the different superconducting properties of the structures the oxygen-deficient regions have been proposed as flux pinning centers [23-25].
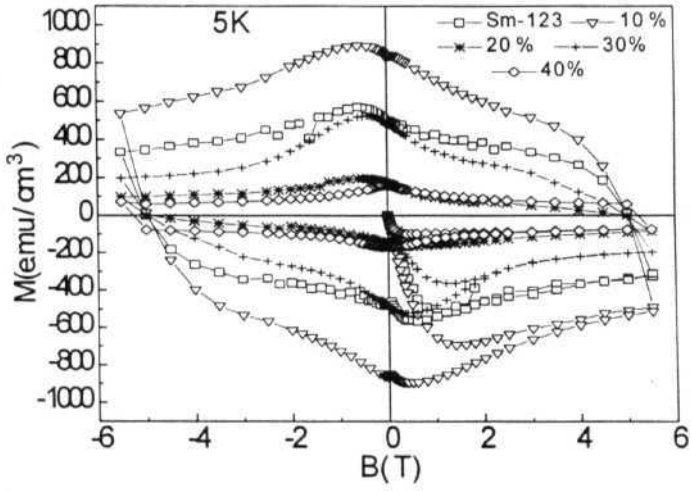
Fig. 3.9(a) : M-H loops of the samples with increasing Sm-211 concentration at 5 K for field applied parallel to c-axis.
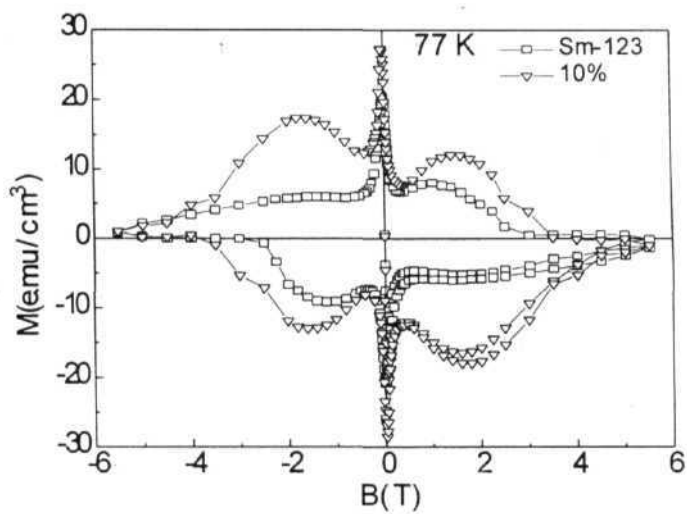
Fig. 3.9(b) : M-H loops of Sm123 and Sm-123 with 10 mol % of Sm-211 at 77 K

for field applied parallel to c-axis.
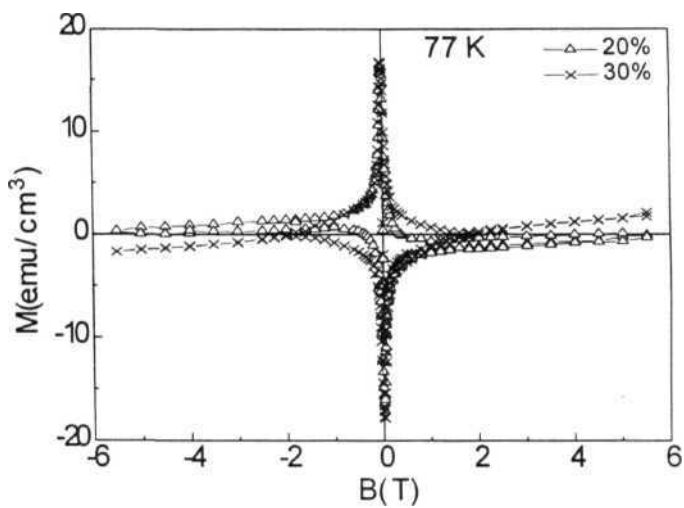
Fig. 3.9(c) : M-H loops of Sm123 with 20 and 30 mol % of Sm-211 at 77 K **for** field applied parallel to c-axis.
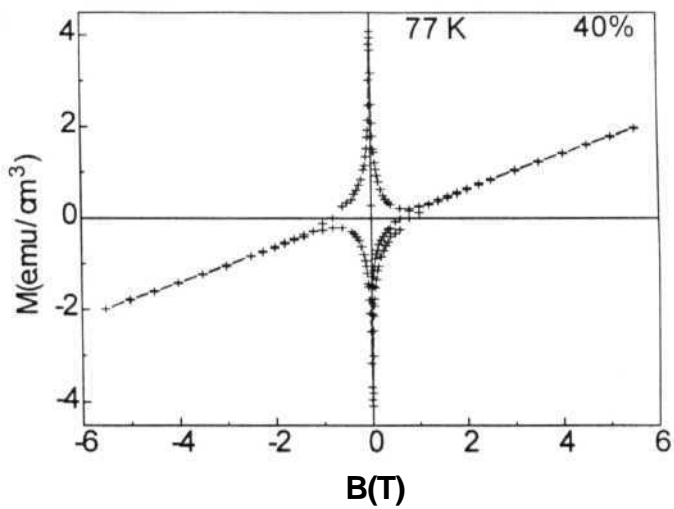
Fig. 3.9(d) : M-H loops of Sm123 with 40 mol % of Sm-211 at 77 K for field applied parallel to c-axis.

3.4. TEM STUDIES

To isolate the origin of the peak-effect in the light rare earth 123s, TEM studies were done on the samples. The 10 mol % sample having a pronounced peak-effect, and the 20 mol % sample having no such effect was selected for the TEM studies. The TEM image (Fig. 3.10(a)) of the 10 mol % sample, at high magnification has micro-twins, stacking faults and dislocations. Fig. 3.10(b) shows the dark field image of the sample which is in contrast to the bright field image of Fig. 3.10(a). This indicates that the features observed are not due any sample artifacts like, thickness, bending of the sample, etc. Though a tweed contrast could not be observed the features within the twins at high magnification, shows a dilute concentration of a second phase. The features present in the TEM images resemble that reported in ref. 22. The exact compositions could not be obtained due to the limitations in the TEM setup. The small area electron diffraction (SAD) pattern within the twin region (Fig. 3.10(c)), did not contain any satellite spots, indicating the absence of modulated structures. The pattern was indexed to the orthorhombic structure of Sm-123, with no spots left unindexed. Fig. 3.10(d) shows the electron diffraction pattern from the second phase present in the sample. As the concentration of the second phase is on a finer scale, faint streaks around the central bright spot are visible in the SAD pattern. The presence of streaks around the central bright spot indicates that the second phase observed in the TEM images is the ortho-II structure. Khachaturyan *el al.* [23] have shown that the presence of diffraction maxima at
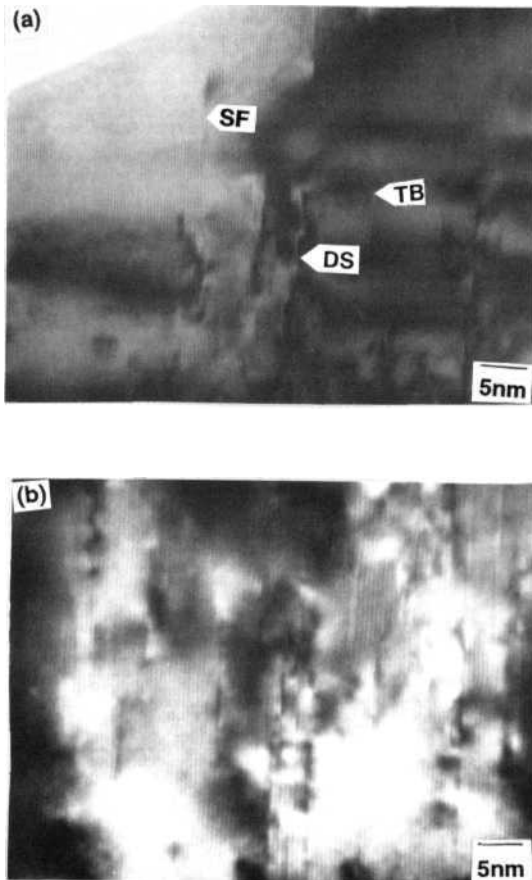
Fig. 3.10. (a) TEM image of the 10 mol % sample at high magnification. TB= Twin Boundary, SF= Stacking Fault, DS= Dislocations.

(b) Dark field image of the sample, the image is a contrast to the Fig. 10 (a).
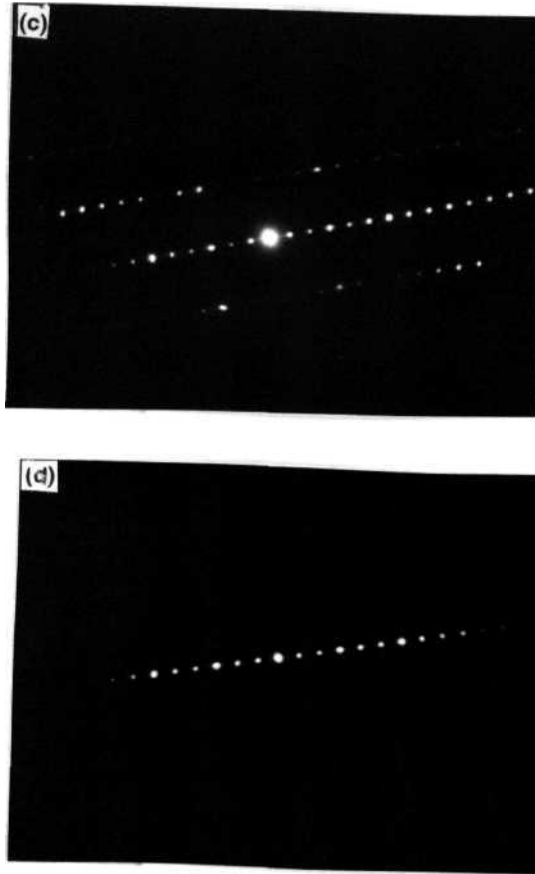
Fig. 3.10. (c) SAD pattern within the twin region of the sample. The zone axis is

[010], and the a- & c- axis lie in the plane of the image.

(d) SAD pattern in a different region of the sample. Faintly visible are streaks

around the central bright spot, due to the fine distribution of the ortho-

II phase.

$1/2\{100\}$ generic points is a feature of the ortho-II structure. It has also been mentioned by them, that if the 123 sample is cooled very slowly while being oxygenated, secondary tweed structure will form within the twins by an oxygen ordering, which will contain the ortho-I and ortho-II structures. The presence of ortho-II structure has been reported in Y-123 by many groups [24], and also in oxygen depleted Y-123 sample [25], in which the oxygen depletion was due to irradiation effect. In the present study on the Sm-123 sample, the possibility of irradiation in the TEM was minimized by using an accelerating voltage of 160 kv, which is below the value which would have irradiated the sample [26]. The ortho - II structure is an oxygen deficient 123 with a doubling of the unit cell [24]. This leads to the conclusion that the two structures present are: ortho-I with a T_c above 90 K and ortho-II structure with a T_c ~ 60 to 90 K. The ortho-II structure in the sample is distributed on a nanometer scale and can be a source of flux pinning at 77 K in high fields, as it turns normal.

In support of the above it may be mentioned that, Khachaturyan *et al.* [27] have reported that it is thermodynamically possible for the 123 phase to decompose 'spinodally' around 500°C during oxygenation. As it passes sequentially through a series of stoichiometric compositions of Magneli-type phases, a cell doubled ortho-II structure having oxygen deficiency will result. Thus it is possible that "spinodal decomposition" into ortho-I and ortho-II structure is also taking place in the LRE-123 systems around 500°C during oxygenation. The idea of field-induced pinning from the low-T_c solid-solution regions may not be valid, the present data did not indicate the presence of such regions. The solid-solution regions will have lower c-

lattice parameter because of the substitution of Ba-atom by rare-earth atom [13]. But in the SAD patterns the values of c-parameters were identical. Also, the solid-solution regions would appear in the SAD pattern as different reflection spots, but no such extra unindexed spots were present.

Similar studies were done on the sample having a starting composition of 20 mol % of Sm-211. The TEM image of this sample shows the presence of twin boundaries (Fig. 3.1 1(a)). Fig. 3.1 1(b) shows the SAD pattern for the sample, and the satellite reflections present in the pattern is indicative of the presence of twins in the sample. The SAD pattern recorded within the twin region is shown in Fig. 3.11(c), the pattern was indexed to orthorhombic Sm-123 phase. The high magnification picture (Fig. 3.1 1(d)) within the twin boundaries do not have a second phase as observed in the 10 mol % sample, but has micro-twins within the twin boundaries. The data clearly shows that a spinodal decomposition is not taking place in the sample containing 20 mol % Sm-211.

It is known that [28], for an oxide alloy to decompose spinodally, the three important controlling parameters are composition of the alloy, the annealing temperature and elastically soft directions of the solid. Variations in any one of them may disallow the spinodal decomposition. In the literature, it is reported that stoichiometric melt processed RE-123 samples and single crystals show the peak-effect, because of the spinodal decomposition during oxygenation. Here it is shown that the 10 mol % 211 sample also exhibits this phenomenon. The sample with 20 mol % 211 is not having the peak-effect because of the absence of the 'spinodal decomposition'. The exact reason for absence of 'spinodal decomposition' in this
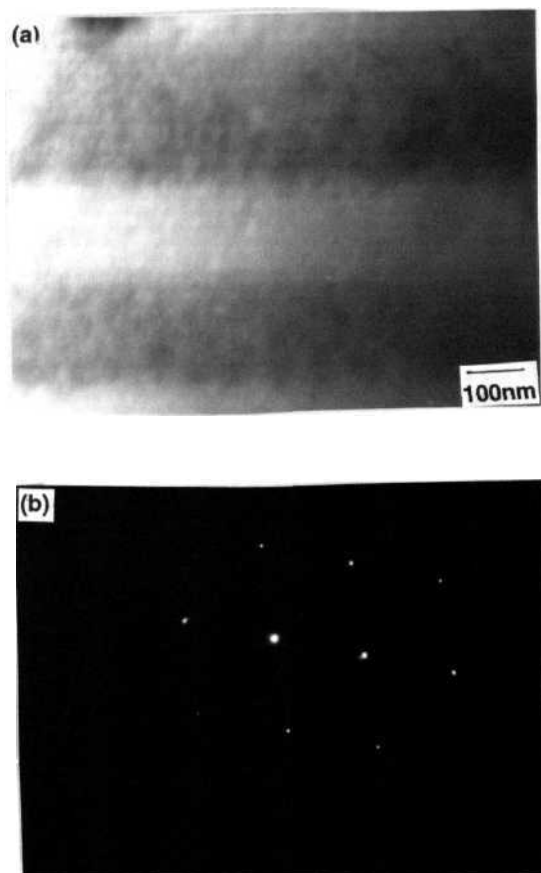
Fig. 3.11. (a) TEM image of the 20 mol % sample showing the twin boundaries in
the sample at low magnification.

(b) SAD pattern of the sample having satellite reflection spots, indicating
the presence of twins in the sample.
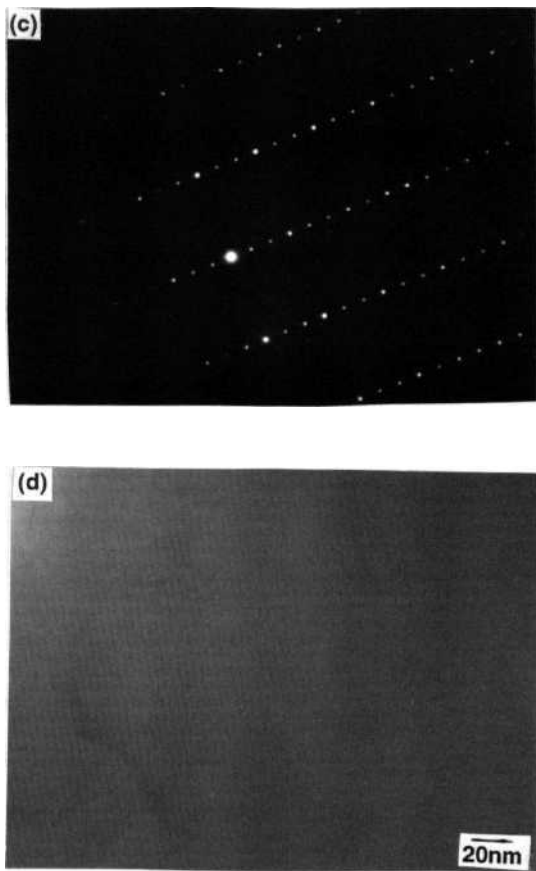
Fig. **3.11.** (c) : SAD pattern of the 20 mol % sample within the twin regions of the

sample, indicating clearly the structure of Sm-123.

(d) : High magnification TEM picture of the sample, having no second

phase   distribution within the twin regions of the sample.

sample is difficult to isolate; because many factors are involved as mentioned above. But the origin of the field-induced pinning contributing to the peak-effect or the fishtail effect **in** the LRE-123 samples is identified to be from the low-T_c oxygen deficient regions, as observed in the Y-123 samples. The oxygen deficient regions

do not contribute to the pinning at low fields and in low temperatures, due to the proximity effect coupling between the ortho-I & ortho-II regions. At high fields and high temperatures, the oxygen deficient regions are driven into their normal state because they posses lower H_{c2} and T_c, than the oxygen rich regions. Those normal regions contribute to flux pinning, resulting in an increase in J_c near such fields at 77 K.

3.5. TEMPERATURE VARIATION OF M-H LOOPS

Fig. 3.12 shows the magnetization hysteresis loop from 60 to 86 K for field applied parallel to c-axis for the samples exhibiting peak-effect. They are Sm-123 and Sm-123 containing 10 mol % Sm-211 labeled in this section as sample No. 1 & 2. Sample No. 2 has a pronounced peak-effect in comparison to No. 1. It is clearly visible that the peak in the M-H loop shifts to low fields with increase in temperature. The peak at 60 K is around 5 Tesla region, and the peak gradually moves to lower fields with increase in temperature. This due to the fact that the low-T_c regions which contribute to pinning become normal at lower fields at higher temperatures.
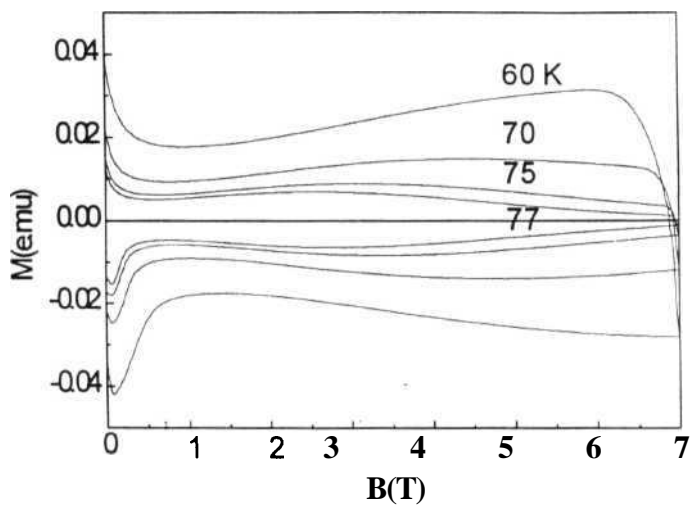
Fig. 3.12(a) : Magnetization hysteresis loop of Sm-123 sample with 10

mol % of Sm-211 from 60 K to 77 K, for field applied parallel to c-axis.
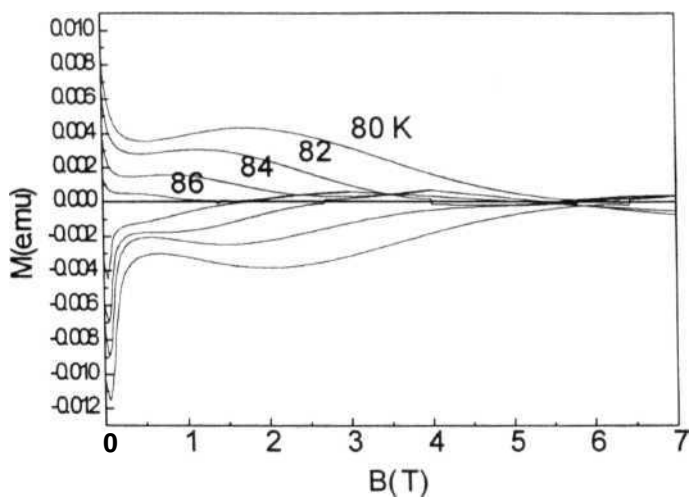
Fig. 3.12(b) : Magnetization hysteresis loop of Sm-123 sample with 10 mol % of

Sm-211 from 80 **K** to 86 **K,** for field applied parallel to c-axis.
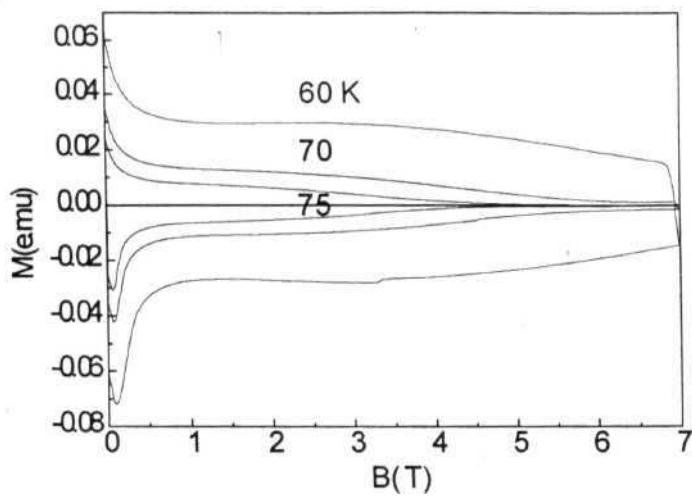
Fig. 3.12(c) : Magnetization hysteresis loop of Sm-123 sample from 60 K to 77 K, for field applied parallel to c-axis.
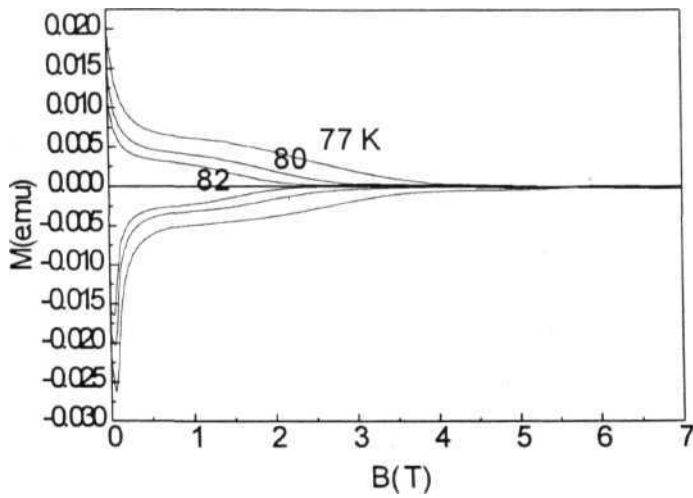
Fig. 3.12(d) : Magnetization hysteresis loop of Sm-123 sample from 77 K to 82 K, for field applied parallel to c-axis.

3.6.   CURRENT DENSITY & FLUX PINNING

In Fig. 3.13 the J_c-H relations are plotted for the samples at different temperatures. The J_c increases for low additions of 211 concentration in the starting material. The 10 mol % sample has a higher J_c than the **stoichiometric** sample. The J_c drops for the 20 mol % sample and again it increases slightly for the 30 mol % sample.
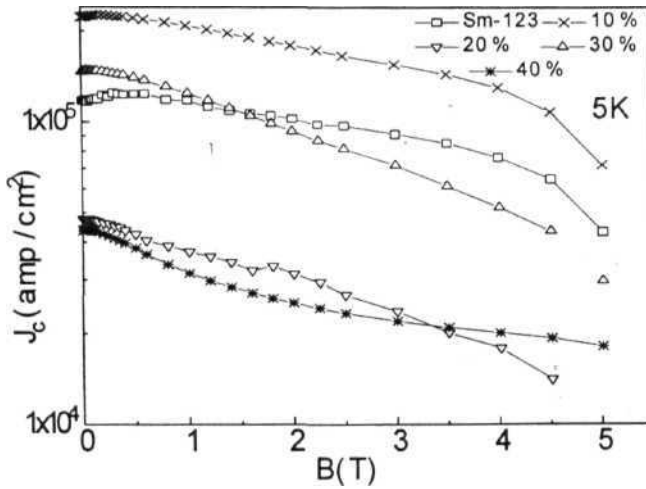
Fig. 3.13(a): J_c-H relations for the samples with increasing Sm-211 content at 5 K.
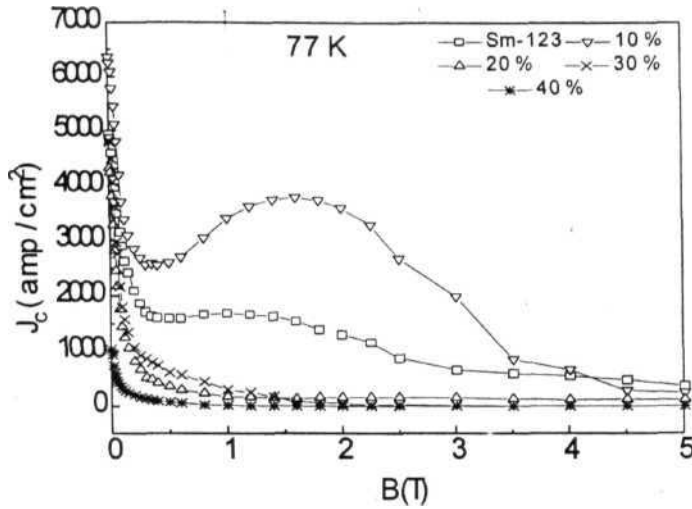
Fig. 3.13(b) : J_c-H relations for the samples with increasing Sm-211 content at 77 K

The 40 mol % sample has a lower J_c than the 30 mol % sample. The J_c at 77 K for 1 Tesla field is plotted in Fig. 3.14, it shows that the J_c has a major peak at the 10 mol % sample and has a minor peak at the 30 mol % sample. It is reported that the J_c in RE-123 (RE= Y to Gd) increases with 211 concentration, and reaches a maximum around 30 mol % of 211 [29,30], for further increase in 211 concentration the J_c drops to lower values due to saturation of the microstructural features. This J_c behaviour was explained from the microstructures of the samples, with increase in 211 concentration the 211 particles were reduced to a smaller size and thus enclosed large amounts of defects. These defects played a crucial role in increasing the J_c. The present experimental results show that the LRE-123 samples

have a different J_c behaviour for increasing 211 concentration. For low additio.

211 concentration the J_c increases due to the presence of field induced pinning from the low-T_c ortho-II regions which seem to play a major part in increasing the J_c. The J_c decreases for the 20 mol % sample because of the absence of field induced pinning. Also the sample is free of crystallographic defects in the matrix, as observed in the TEM images. The second minor peak in J_c is at 30 mol %, which can be due to the optimal refinement of 211 particles in the microstructure. The small sized 211 particles may be surrounded by crystallographic defects like stacking faults etc, which may had increased the J_c, like in the RE-123 case. However, the J_c increase for 30 mol % as observed in the Y-123 samples is not present here. The J_c at zero fields is higher for the samples with high concentration of 211, but it reduces to low values with increase in field. The J_c-H behaviour with increase in 211 concentration for Nd-123 melt textured samples is reported to be similar [31], as observed in our experiments. This leads to the conclusion that the J_c-H behaviour with increase in 211 concentration for LRE-123 melt textured samples is different incomparison to other RE-123 samples.

The pinning force is calculated using the relation $F_p = J_c B/10$, and is plotted against the field in Fig. 3.15. The figure shows that the pinning force is higher for the stoichiometric and the sample containing 10 mol % Sm-211 sample. The samples containing 20, 30 & 40 mol % of Sm-211, have very low pinning force. The higher pinning force in the samples with low 211 concentration is because of the reason given above.
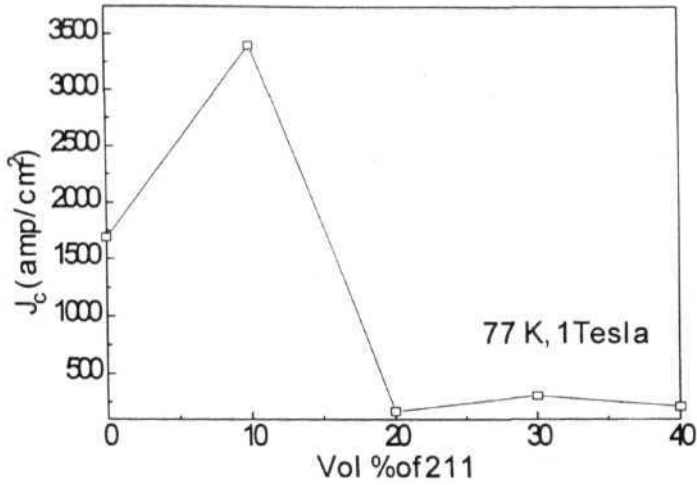
Fig. 3.14 : J_c at 1 Tesla field at 77 K for the samples vs the mol percentage of added 211 concentration.

The experimental results indicate that addition of an optimum 211 concentration (around 10 mol %) in the LRE-123 enhances J_c, and for higher concentration it reduces to low values. This result is different to the reported values of concentration required to enhance J_c in RE-123 melt textured samples, where an addition of 30 mol % enhanced the J_c.

The pinning force for the two samples (Sm-123 and Sm-123 with 10 mol % Sm-211) showing the peak-effect is plotted against the field from temperatures of 4 K to 80 K in Fig. 3.16. The figure shows that the Sm-123 sample (sample 1) has a higher pinning force than sample with 10 mol % Sm-211 (sample 2) in the temperatures below 60 K. Above 60 K sample 2 has a higher pinning force in

comparison to sample 1. The data confirms that the oxygen deficient regions are responsible for the anomalous pinning in the M-H loop, as it enhances the J_c and pinning force above 60 K and below T_c in high fields.
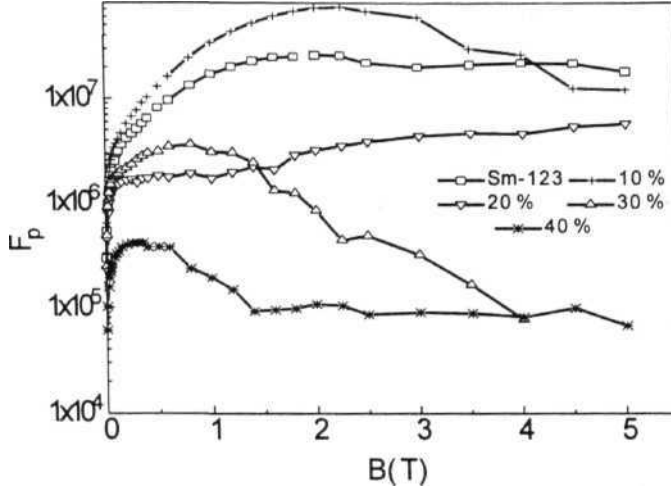
Fig. 3.15 : Variation of the flux pinning force with field for the samples with increasing Sm-211 content at 77 K.
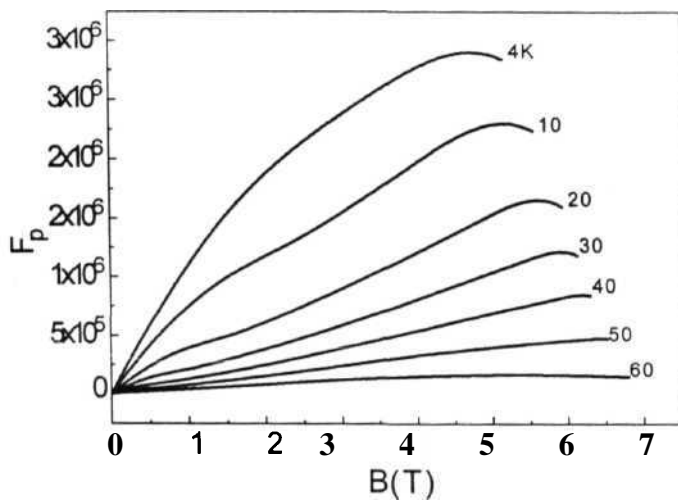
Fig. 16(a) : Flux pinning force of sample 1 (Sm-123) from the temperatures 4K. to 60 K.
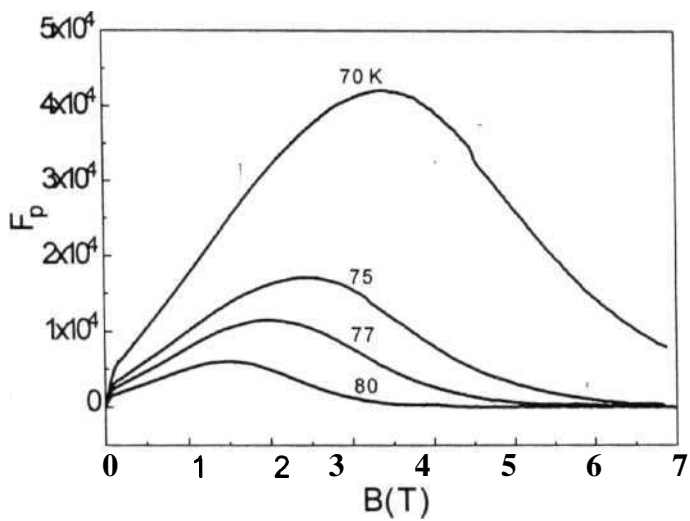
Fig. 16(b): Flux pinning force of sample 1 (Sm-123) from the temperatures 70K to 80 K.
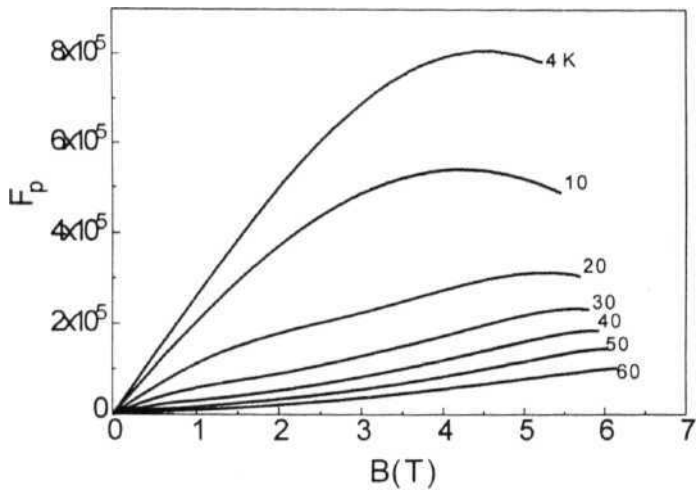
Fig. 16(c) : Flux pinning force of sample 2 (Sm-123 with 10 mol % Sm-211) from the temperatures 4K to 60 K.
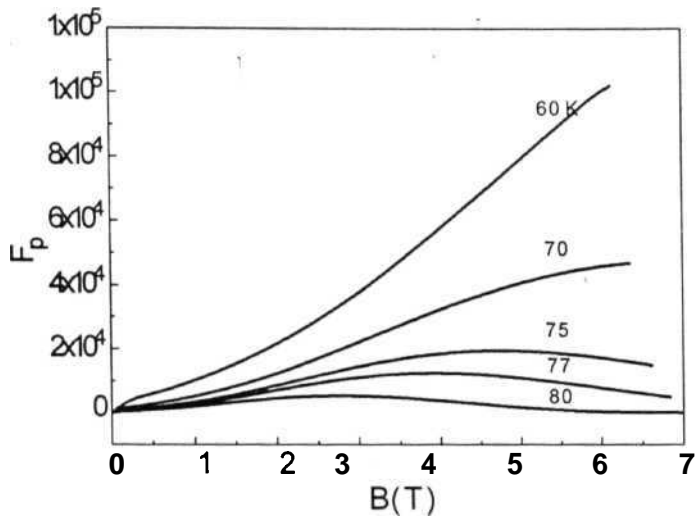
Fig. 16(d) : Flux pinning force of sample 2 (Sm-123 with 10 mol % Sm-211) from the temperatures 60 K to 80 K.

3.7.   IRREVERSIBILITY LINE

The irreversibility line (IR line) divides the region below which the properties are reversible that which they are irreversible. The slope of the IR line is an indication of the pinning strength. For higher pinning strength, the slope will be much steeper [32]. Fig. 3.17 shows the IR line for the two samples. Sample 2 has a higher slope (-0.69) than sample 1 (-0.46) in the temperature range of 70-90 K. This indicates that the pinning strength has enhanced in that temperature range, due to the presence of the field induced pining as discussed above. This result is in agreement with the above calculated pinning force, which showed a higher pinning strength for sample 2 above 70 K. The IR line has a point of inflection above which the slope changes to a much higher value. The features of it will be discussed in the next section.

3.8. NORMALISED CREEP RATE

The magnetic relaxation is important as it sets limits to the stability of superconducting devices. The current density of a superconducting sample is dominated by pinning in low fields and relaxation in the high fields. The normalised relaxation rate eliminates the fundamental parameters, and is directly derived from measurements of dM/d(lnt) ([33] and the references in that review). The variation of normalised relaxation rate with field at 77 K is plotted in Fig. 3.18 for the two samples. The relaxation rate of sample 1 increases with field, and for sample 2 the relaxation rate decreases to a very low value in the 1-2 Tesla region, and thereafter increases with field. The value of the field at which the minimum in

the relaxation rate has reached (1.2 T), is equal to the field value at which the slope of the IR line changes to a higher value. In Fig. 3.19, the J_c, flux pinning force and relaxation rate, at 77 K for sample 2 are plotted together. It shows that the field at which the peak in J_c is obtained is not coincident with the value at which there is a drop in the relaxation. The field value at which the peak in J_c is obtained is approximately equal to double the value at which a minimum in relaxation rate has reached. The flux pinning force has a peak around 4 Tesla. This indicates that a saturation of pinning is taking place at that field value, above that field value the relaxation mechanism dominates and below it the pinning mechanism plays an important role. It also indicates that the peak in the hysteresis loop is not due to a decrease in the relaxation rate. The alternative is to consider the field induced pinning from oxygen deficient regions.

In Fig. 3.20, the J_c , pinning force and relaxation rate at 77 K for sample 1 are plotted together. It can be seen that as the relaxation rate increases the J_c decreases. Also, wherever there is a slope change in the relaxation rate, correspondingly there is a drop in the J_c at same field value. Initially the relaxation rate drops because the flux has to enter the specimen and has to get redistributed. During this the relaxation drops to a low value. The relaxation rate then increases linearly with field. At a field of 0.9 Tesla there is slope change, this corresponds to the field at which there is a slope change in the IR line. The slope of the relaxation rate again changes at a field value of 2.3 Tesla, this corresponds to the peak in the flux pinning force. A saturation of pinning takes place at this field value and above it the relaxation completely dominates and it increases linearly. Fig. 3.19 and 3.20 clearly indicate that in low fields the behaviour of J_c is dependent on pinning and in

high fields the relaxation mechanism dominates it. The low relaxation rate at 77 K for sample 2 in comparison to sample 1, is due to the predominance of field induced pinning from the low T_c oxygen deficient regions. The drop in relaxation rate and a steeper IR line help to operate the superconducting devices at higher temperatures and fields. This is because sustainable current density can be maintained even under those conditions. But it is difficult to tailor make a sample with the required amount of defects. Irradiation of the sample might help to further lower the relaxation rate as it produces columnar defects of a smaller dimension [34].
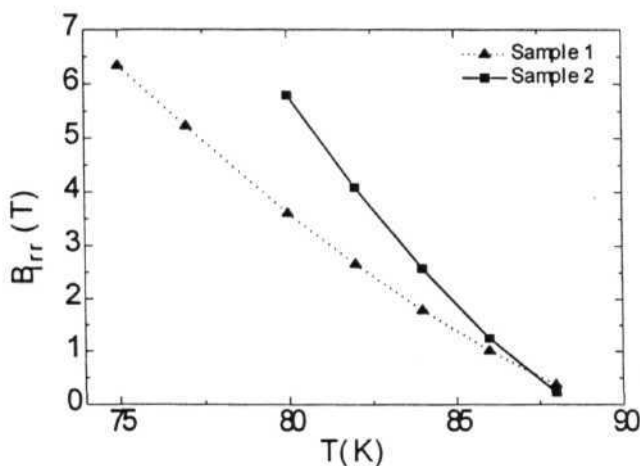
Fig. 3.17: Irreversibility line for samples 1 and 2 for field applied parallel to c-axis.
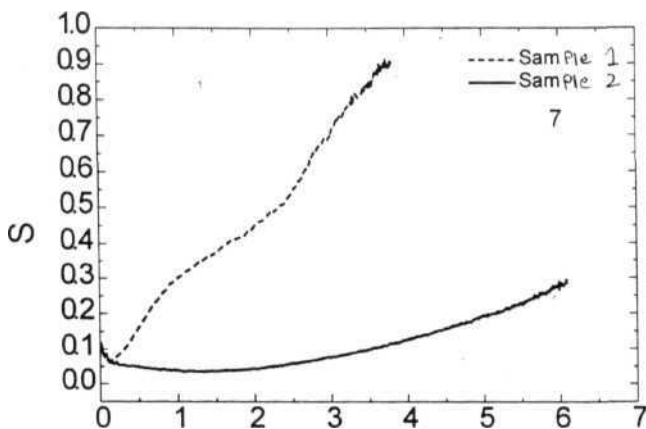
Fig. 3.18 : Variation of the normalised relaxation rate with field at 77 K for the samples 1 & 2.
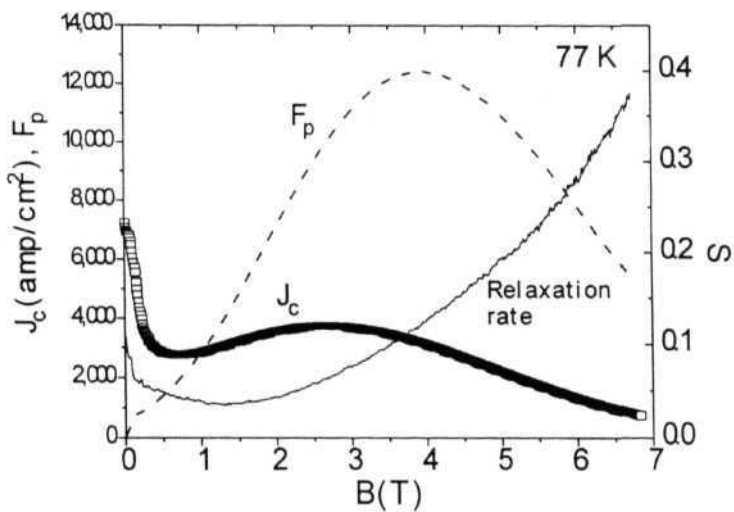
Fig. 3.19 : Plot of J_c, pining force and relaxation rate with field for sample 2 at 77 K.
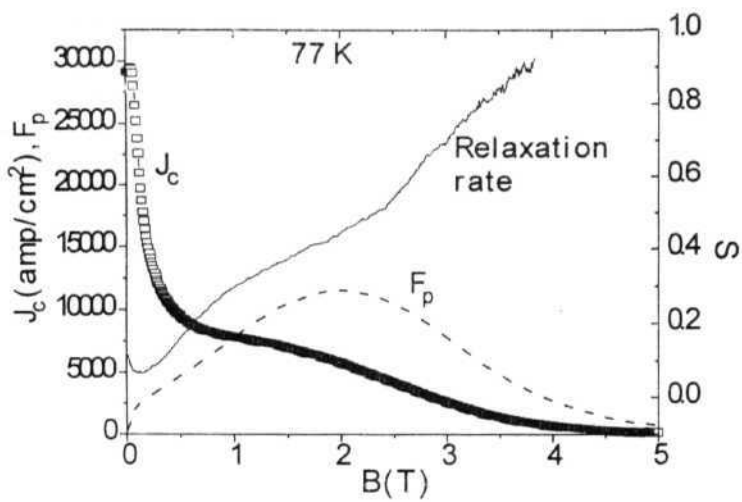
Fig. 3.20 : Plot of J_c, pinning force and relaxation rate with field for sample 1 at 77
K.

REFERENCES

1.a S. Jin, T. H. Tiefel, R. C. Sherwood, R. V. van Dover, M. E. Davis, G. W. Kammlott, and R. A. Fastnacht, Phys. Rev B 37, 7850 (1988).

1.b. K. salama, V. Selvamanickan, L. Gao, and K. Sun, Appl. Phys. Lett. 54. 2352 (1989).

1.c. M. Muralkami, M. Morita, K. Doi, and K. Miyamoto, Jpn. J. Appl. Phys. 28, 1189(1989).

2. A. Goyal, K. B. Alexander, D. M. Kroeger, P. D. Funkenbusch, and S. J. Burns, Physica C 210, 197 (1993).

3. M. Mironova, D. F. Lee and K. Salama, Physica C 211., 188 (1993).

4. M. Murakami, , S. Gotoh, N. Koshizuka, S. Tanaka, T. Matsushita, S. Kambe, and K. Kitazawa, Cryogenocs 30, 390 (1990).

5. P. McGinn, P. McGinn, N. Zhu, W. Chen, S. Sengupta, and T. Li, Physica C 176.   203(1991).

6. S. Jin, T. H. Teifel, and, G. W. Kammlott, Appl. Phys. Lett §9, 540 (1991).

7. D. F. Lee, V. Selvamanickam, and K. Salama, Physica C 202, 83 (1991).

8. C. J. Kim, K. B. Kim, I. S. Chang, D. Y. Won, H. C. Moon and D. S. Shur, J. Mater. Res. 8,699 (1993).

9. H. Fujimoto, M. Murakami, T. Omaya, Y. Shiohara, N. Koshiuka and S. Tanaka, Physica C 203, 103 (1992).

10. D. Shi, S. Sengupta, J. S. Lou, C. Varanasi and P. J. McGinn, Physica C 213. 179(1993).

11. S. I. Yoo, M. Murakami, T. Higuchi, N. Sakai, J. Weltz, N. Koshizuka and S. Tanaka, Jap. J. Appl. Phys. 33, L715 (1994).

12. F. Garcla-Alvarado, E. Moran, M. Vallet, J. M. Gonzalez-calbet, M. A. Alario, M T. Perez-Frias, J. L. Vicent, S. Ferrer, E. Garcia-Michel and M. C. Asensio, Solid. State Comm. 63, 507 (1987).

13. M. Sano, Y. Hayakawa and M. Kumazawa, Sup. Sci & Tech 9, 478 (1996).

14. "*Melt Processeed High-Temperature Superconductors*" ed. M. Murakami, World Scientific, Singapore, (1992).

15. Hai-Wong park,, K. B. Kim, K. W. Lee, H. Kuk, G. W. Hong and C. J. Kim, Sup. Sci & Tech 9, 694 (1996).

16. "*Interpretation* of Metallographic Structures", W. Rostoker, Acad. Press.,P.213.

17. R. Goplan. T. Roy, T. Rajasekharan, G. Rangarajan and N. Hari Babu, Physica C 244, 106(1995).

18. Z. L. Wang, A. Goyal and D. M. kroeger, Phys. Rev. B 47, 5373 (1993).

19. E. Sudhakar Reddy and T. Rajasekharan (Communicated).

20. M. Murakami, S. I. Yoo, T. Higuchi, N. Sakai, J. Weltz, N. Koshizuka and S. Tanaka, Jap. J. Appl. Phys. 33, L1000 (1994).

21. T. Egi,, J. G. Wen, K. Kuroda, H. Unoki and N. Koshizuka, Appl. Phys. Lett, 67,2406(1995).

22. M. Nakamura, T. Hirayama, Y. Yamada, Y. Ikuhara and Y. Shiohara, Japn. J. Appl. Phys. **35**, 3882 (1996).

23. J. L. Vargas & D. C. Larbalestier, Appl. Phys. Lett. 60, 1741 (1992).

24. M. Daumeling, J. M. Seuntjens & D. C. Larbalestier, Nature **346,** 332 (1990).

25. J. Vancken, E. Osquiguil, & Y. Bruynseraede, Physica C **183,** 163 (1991).

26. C. P. Brumster, S. Quong, L. T. Wille, R. Gronsky, B. T. Ahn, V. Y. Lee, R. Beyers, T. M. Gur, & R. A. Higgins, Mat. Res. Symp, **183,** 369 (1990).

27. A. G. Khachaturyan, Phys. Rev. Lett. 61, 215 (1988).

28. R. W. Cahn, Trans. Met. Soc. AIME 252, 166 (1968).

29. Murakami, H. Fujimoto, S. Gotoh, K. Yamaguchi, N. Koshizuka, and S. Tanaka, Physica C **185-189**, 321 (1991).

30. E. Sudhakar Reddy and T. Rajasekharan, (Communicated).

31. M. Murakami, N. Sakai, T. Higuchi and S. I. Yoo, Sup. Sci. & Tech, 9, 945 (1997).

32. M. Slaski, L. T. Sagdahl, L. K. Heill, K. Fossheim, M. Murakami, H. Fujimoto, N. Koshizuka and S. Tanaka, Sup. Sci. & Tech **5,** S340 (1992).

33. Y. Yeshrun, A. P. Malozemoff, A. Shaulov Rev. Mod. Phys. 68, 911 (1996).

34. K. Salama and D. F. Lee, Sup. Sci. & Tech. 7, 177 (1994).

CHAPTER IV

REFINEMENT OF <u>Sm-211</u>

4. 1. INTRODUCTION

Melt texturing of 123 phase using the peritectic reaction is an effective method for obtaining high J_c in the bulk materials [1-3]. The high J_c is because of alignment of 123 grains in the **ab-plane,** and reduced number of weak links. The 123/211 interface encloses many crystallographic defects which enhance the flux pinning and increase the J_c [4]. The characteristics of the 123/211 interface and the morphology of 211 precipitates vary with the processing methods. A critical size, morphology and an optimum volume percentage of 211 in the **microstructure** is essential for obtaining high J_c.

The important parameters for producing **fine** sized 211s are control over nucleation of 211s at the peritectic melting stage of 123 phase, and low coarsening effect of 211 particles during the melt processing. Taking excess of 211 phase in the starting material and modifications in the heating schedule yield **fine** sized 211s [5]. Also, the 211 addition produces a homogeneous 123 microstructure by removing any liquid phase residual from incomplete peritectic reaction, and suppresses the formation of macro-cracks during the heating cycles [6]. An alternative method to get refined 211s is by additions like PtO_2, CeO_2, etc. These additions have been suggested

to suppress the coarsening of 211s in the liquid phase and to change the morphology of 211s [7-10].

It is observed [11] in melt processed Sm-123 system with increasing Sm-211 concentration in the starting material, that the microstructural features saturate at 30 mol % Sm-211 content, and the average 211 particle size is around 5 urn. The J_c with increasing Sm-211 content has a major peak at the 10 mol % concentration, and a minor peak at 30 mol % 211 content [11]. In the samples with low 211 content (i.e., upto 10 mol %), an additional field induced pinning from the low-T_c oxygen deficient regions plays an important role in increasing the J_c [11]. However, the field induced pinning from the low-T_c regions is absent in the samples with high 211 content (i.e., above 20 mol %) [12]. An increase in 211 content beyond 30 mol % does not reduce the 211 size. The J_c decreases for still higher 211 content because the causative microstructural factors such as 211 size refinement saturates, and the volume of the superconducting fraction decreases. Further refinement of 211 particles cannot be achieved by increasing the 211 content. In order to further refine the 211 particles in the microstructure, samples of Sm-123 with 30 mol % Sm-211 are melt processed with additions like CeO_2, ZrO_2, PrO_2, & Ag. In this chapter, the microstructure and the J_c dependence on field in melt textured Sm-123 sample, for small additions (0.5 wt %) of Ag, CeO_2, ZrO_2 & PrO_2 is discussed. The sample has a starting composition of excess 30 mol % Sm-211, and is prepared in low oxygen atmospheres, to suppress the solid-solution formation. The processing details are mentioned in the earlier experimental chapter.

4.2. PRELIMINARY CHARACTERIZATION

The X-ray diffraction patterns (Fig. 4.1) recorded from the samples are indexed to the orthorhombic 123 phase with some amount of 211 phase. In the XRD pattern, peaks representing the added compounds were not observed. The a, b, c-lattice parameters corresponding to the unit cell closely matched the standard Sm-123 values [15]. This indicates that the solid-solution formation is suppressed in the bulk of the material. Fig. 4.2 shows the resistivity versus temperature plots of the samples. The T_c's are above 90 K, confirming the absence of solid-solution formation in the bulk of the material.

4.3. MICROSTRUCTURE

The SEM pictures (Fig. 4.3) of the samples show that they have the usual features of melt processed samples [16]. Platelets of 123 are aligned parallel with 211 inclusions distributed in them. Some 211-free regions are also seen in the microstructures. The morphology of 211s is circular for all the samples. The spherical morphology of 211s is due to excess 211 phase in the starting material, which refines the 211 particles by providing extra nucleation centers at the peritectic melting stage [17,18]. The additions like CeO_2, etc.. further refine the 211s because, they serve as additional nucleating centers for the 211 phase formed by the peritectic melting of 123 phase. These additions have been proposed to reduce the coarsening behaviour of 211s in the liquid phase [7-10,19], and also reduce the energy for nucleation of fine sized 211s.
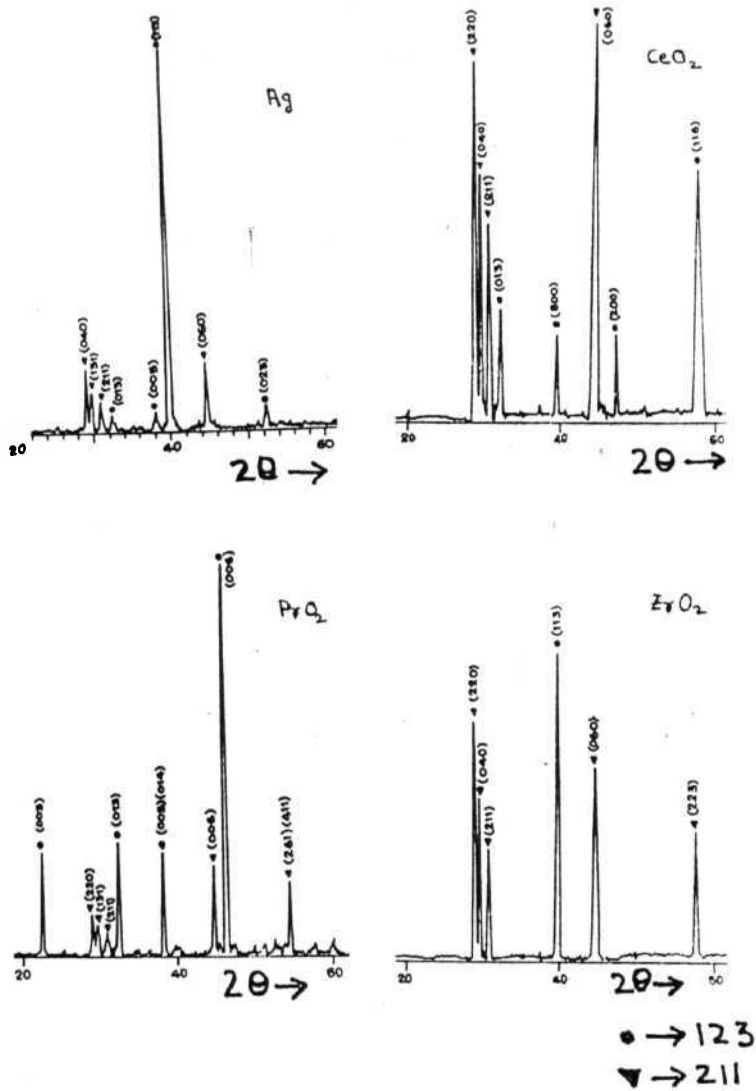
Fig. 4.1 : X-ray diffraction patterns of the samples with additions of (a) Ag, (b) CeO_2, (c) PrO_2 and (d) ZrO,.
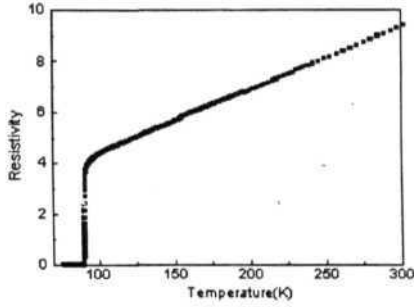
Fig. 4.2(a) : Resistivity vs temperature plot of the Ag added sample. The T_c of the
sample is 91.2 K.
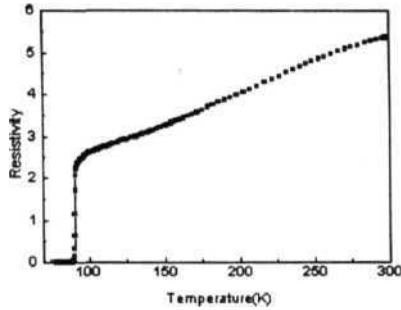
Fig. 4.2(b) : Resistivity vs temperature plot of the CeO_2 added sample. The T_c of
the sample is 91.0 K.
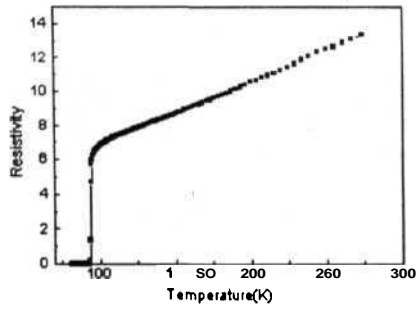
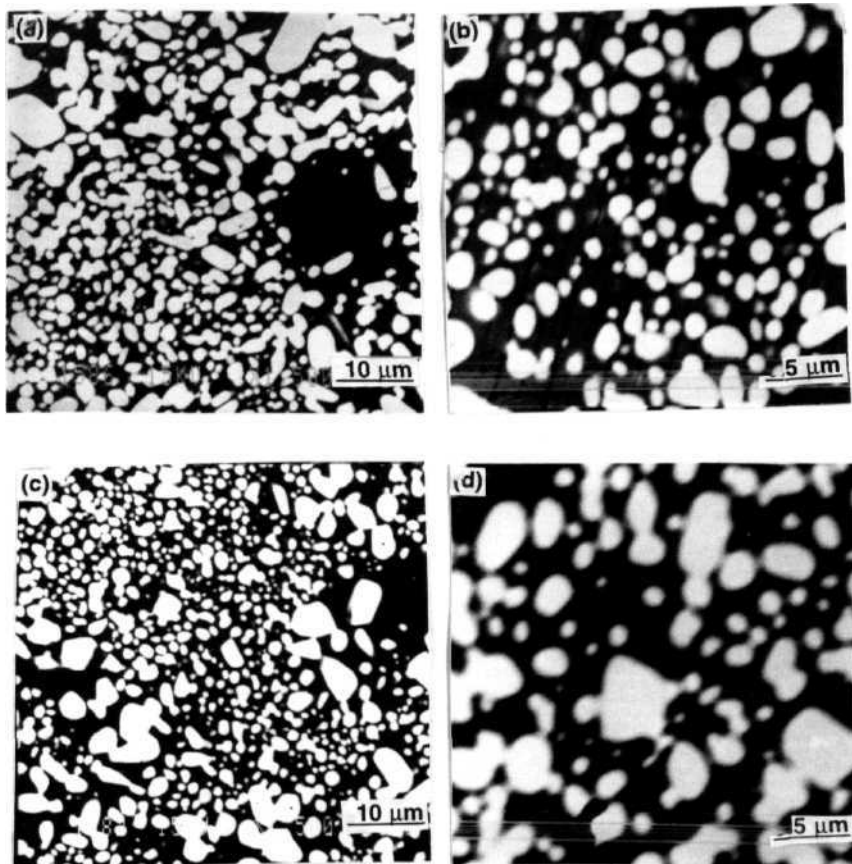Fig. 4.2(c): Resistivity vs temperature plot of the PrO$_2$ added sample. The T$_c$ of the sample is 91.1 K.
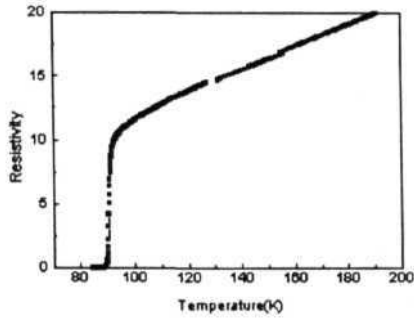
Fig. 4.2(d) : Resistivity vs temperature plot of the ZrO$_2$ added sample. The T$_c$ of the sample is 91.1 K.

Fig. 4.3 : SEM images of the samples with additions of (a) Ag, (b) CeO_2, (c) PrO_2 and (d) ZrO_2.

The 211 particle size distribution in the microstructures indicates that good refinement of 211 particles can be achieved by the addition of a small amount of PrO_2, CeO_2 and ZrO_2. However, among the samples processed, the PrO_2 added sample has a high concentration of sub-micron sized 211s indicating that excellent

refinement can be achieved with this addition. The silver containing sample has finer 211 particles incomparison with the sample without this addition (Fig. 3.4).

However, the 211 particles are of larger dimension in comparison to the samples having other additions. This probably has to do with the fact that Ag is in molten state at the peritectic melting stage; it does not then provide additional nucleating centers. It is reported in the literature that Ag addition to Y-123 reduces the inter platelet gaps formed during melt processing and also refines the 211 particles [10,20].

4.4. dc MAGNITIZATION STUDY

The magnetization hysteresis (M-H) loops are recorded at 25, 50 & 77 K, for field applied normal to the sample surface (Fig. 4.4). No anomalous features like fishtail or peak-effect is observed in the hysteresis loops. The loops were fitted to the generalised critical state model (GCSM) [21], where the J_c has a functional form J_c - $J_o / (1+B/B_o)^n$, the constants J_o, B_o and n are field independent parameters. Reasonable fits were achieved for 25 K and 77 K loops (Fig. 4.5). At 50 K the loops could not be fitted properly to this model. The exponent 'n' used for fitting is tabulated in Table I, it shows that for the CeO_2 added sample 'n' is the least among all the samples, indicating higher pinning strength in the sample. The M-H loops at

50 K were fitted to the Kim's model [22]. Fig. 4.6 shows the loops generated theoretically, in which reasonable fitting was achieved for all the loops, except for the PrO_2 added sample. The M-H loop for that sample did not fit properly to this model also.
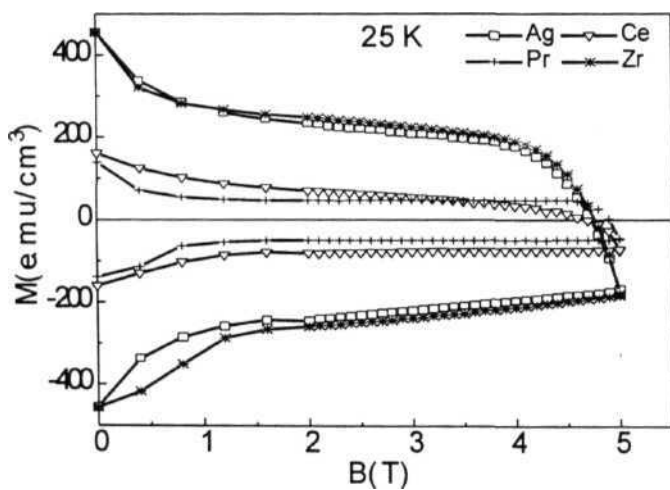
Fig. 4.4(a) : Magnetization hysteresis plots of the sample containing additions of Ag, CeO_2, PrO_2 and ZrO_2, recorded at 25 K.
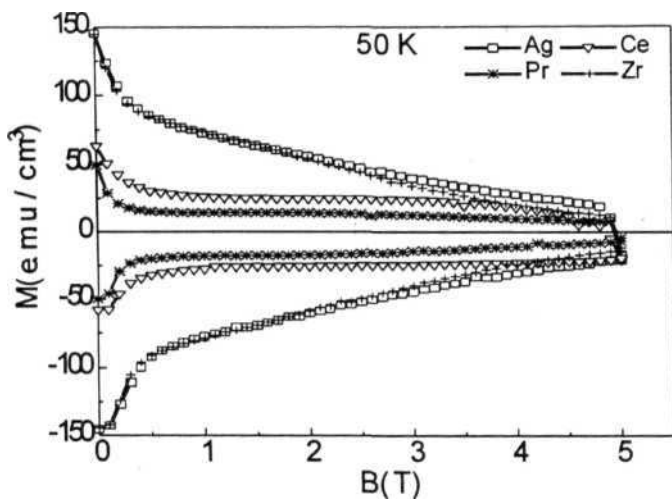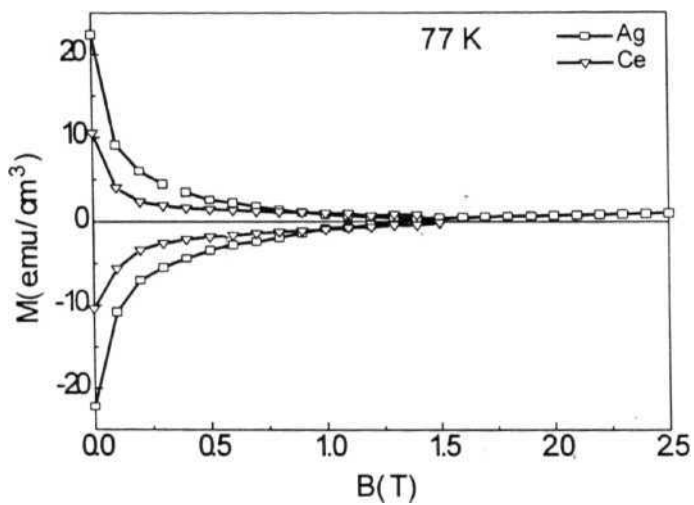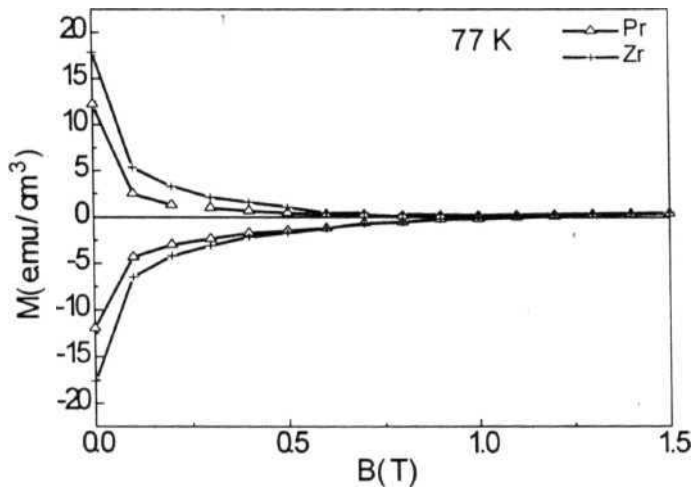
Fig. **4.4(b)** : Magnetization hysteresis plots of the sample containing additions of Ag, CeO_2, PrO_2 and ZrO_2, recorded at 50 K.

Fig. 4.4(c) : Magnetization hysteresis plots of the sample containing additions of

Ag and CeO_2 recorded at 77 K.

Fig. 4.4(tl) : Magnetization hysteresis plots of the sample containing additions of

PrO$_2$ and ZrO$_2$, recorded at 77 K.
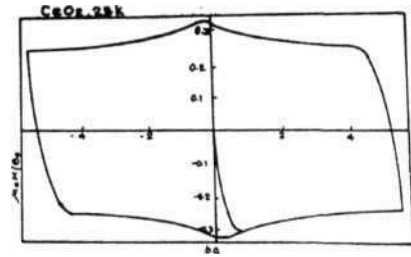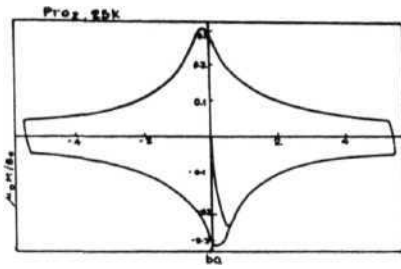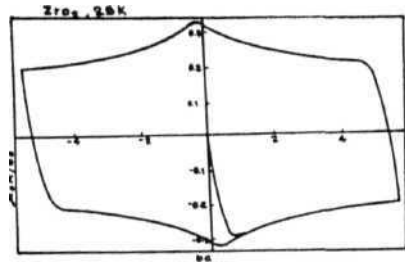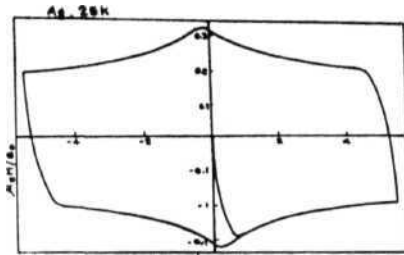
Fig. 4.5 : Fittings to the M-H loops using the generalised critical state model, at 25

K and 77 K.

Fig. 4. 5 : Cotnd..

Fig. 4. 5 : Cotnd..
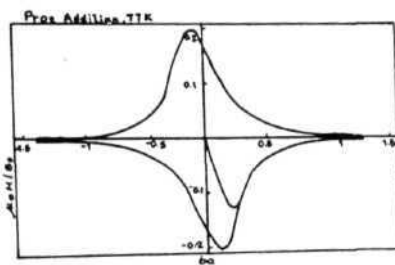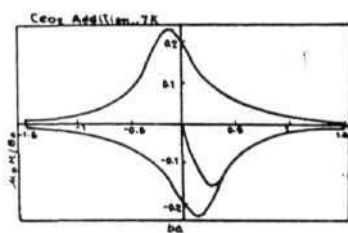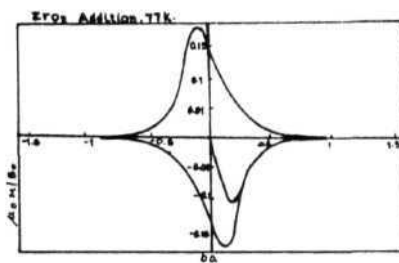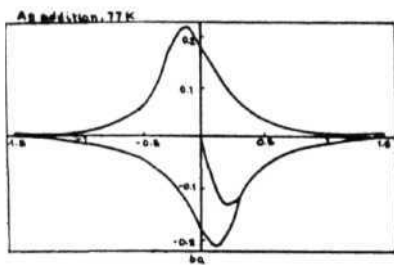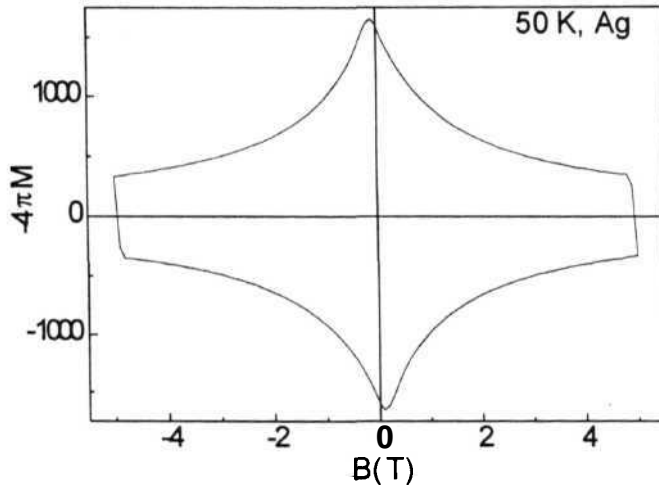
Fig. 4.6(a): M-H loop at 50 K, generated theoretically using the Kim's model for the Ag added sample. $H_p = 0.53$ T, p = 1.05 are the fit parameters.
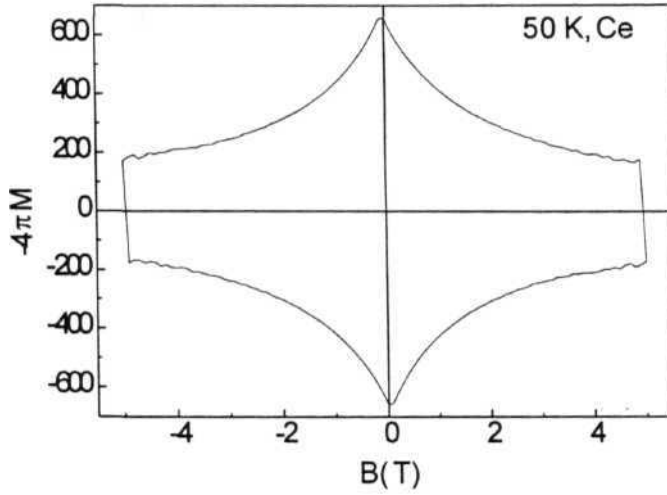
Fig. **4.6(b)** : M-H loop at 50 K, generated theoretically using the Kim's model for the CeO_2 added sample. H_p = 0.24 T, p = 0.5 are the fit parameters.
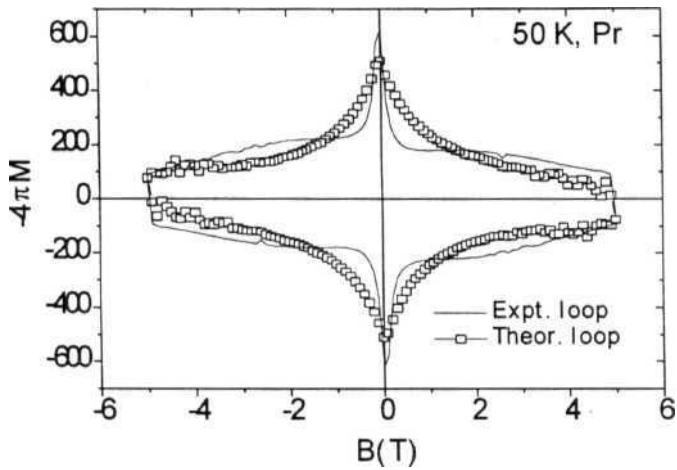
Fig. 4.6(c) : Experimental, and theoretically generated M-H loop at 50 K using the Kim's model for the PrO_2 added sample. H_ρ = 0.12 T, p = 0.56 are the fit parameters
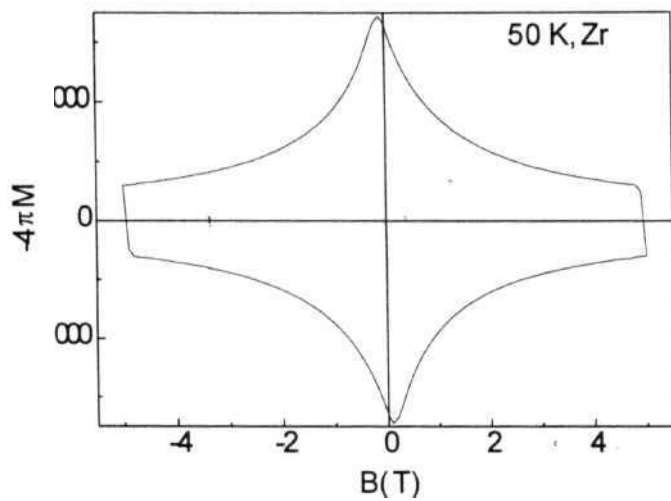
Fig. 4.6(d) : M-H loop at 50 K, generated theoretically using the Kim's model for

the ZrO_2 added sample. H_p = 0.42 T, p = 1.04 are the fit parameters.

4.5. CURRENT DENSITY & FLUX PINNING

The J_c was estimated using Bean's model, and the field dependence of it is plotted in Fig. 4.7. The data shows that there is an increase in J_c by a factor of two for the samples with the additions, incomparison to the sample without these additions for the same amount of Sm-211 concentration in the starting material (Fig. 4.7(d)) [11]. The Ag added sample has a higher J_c and the best field dependence of J_c. The J_c behaviour of the ZrO_2 added sample closely matches that of the Ag added sample. Inspite of having a large concentration of fine

sized 211's in the microstructure, the J_c and its field dependence of CeO_2 and PrO_2 added sample is relatively poor. The T_c of the CeO_2 and PrO_2 added samples are almost the same as the other samples, but the J_c is low. This may be due to the reactivity of those additions with the parent phase. The high J_c in Ag added sample has to do with the reduction of crack formation during melt processing [10, 20].

The pinning force is calculated for the samples at 77 K, using the relation F_p = J_c B. The variation of the normalised pinning force (F_{pmax}), with field is plotted in Fig. 4.8. It shows that, at 77 K the sample with CeO_2 addition had a higher pinning force in comparison to the other samples. Fig. 4.9 shows the variation of normalised pinning force with field, where b= B/B*, and B* is the maximum applied field. All the samples have a similar behaviour, and exhibit a peak around 0.2, indicating that the pinning mechanism is due to dislocations [23]. The CeO_2 added sample had a peak around 0.6, the pinning here is also due to the dislocations as the peak

signifying this pinning mechanism will be between 0.25 and 0.85, and the peak

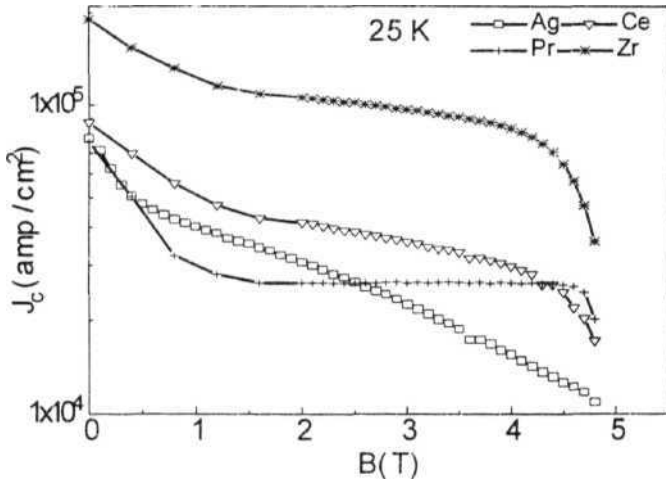signifying the pinning from precipitates or plane boundaries will be around 0.3 [23].

Fig. 4.7(a) : J_c-H plots of the samples containing additions of Ag, CeO_2, PrO_2, and
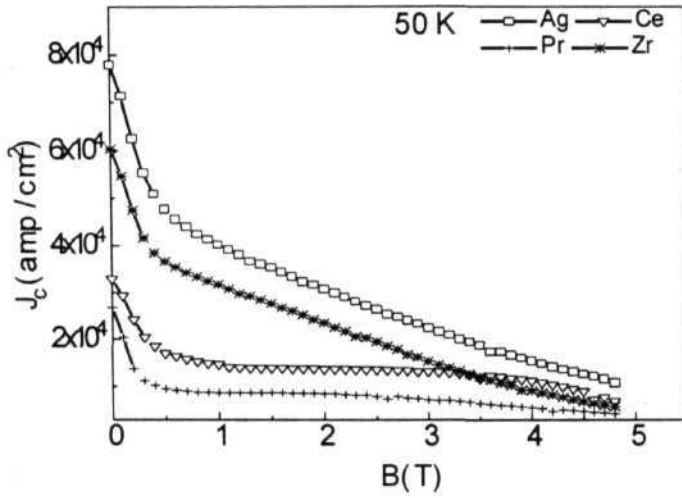
ZrO, at 25 K.

Fig. 4.7(b) : J_c-H plots of the samples containing additions of Ag, CeO_2, PrO_2, and
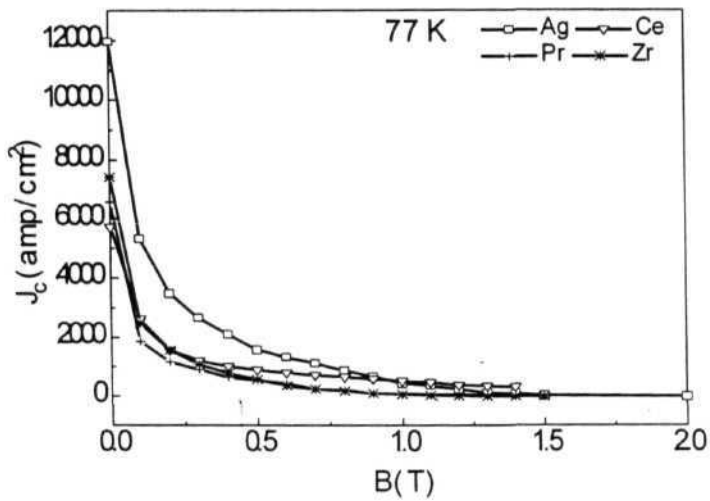
ZrO_2 at 50 K.

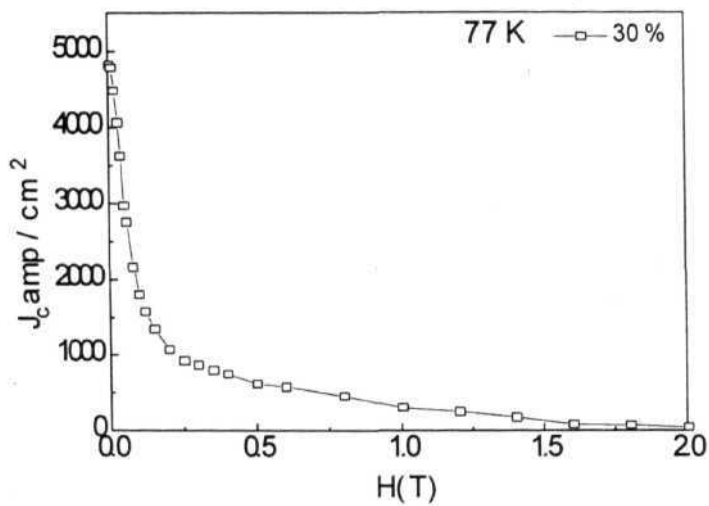Fig. **4.7(c)** : J_c-H plots of the samples containing additions of Ag, CeO_2, PrO_2, and ZrO_2 at 77 **K**.

Fig. 4.7(d): J_c-H plot of the Sm-123 + 30 mol % Sm-211 sample at 77 K.
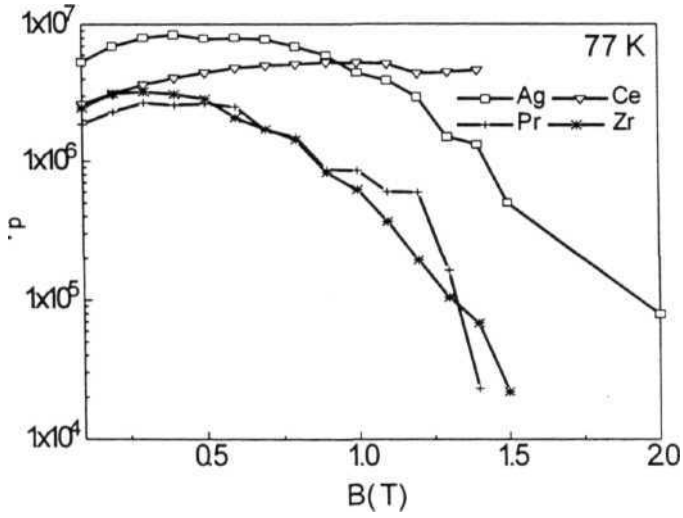
Fig. 4.8 : Plot of the **flux** pinning force (F_p) vs the field at 77 **K,** for the samples with the additions.
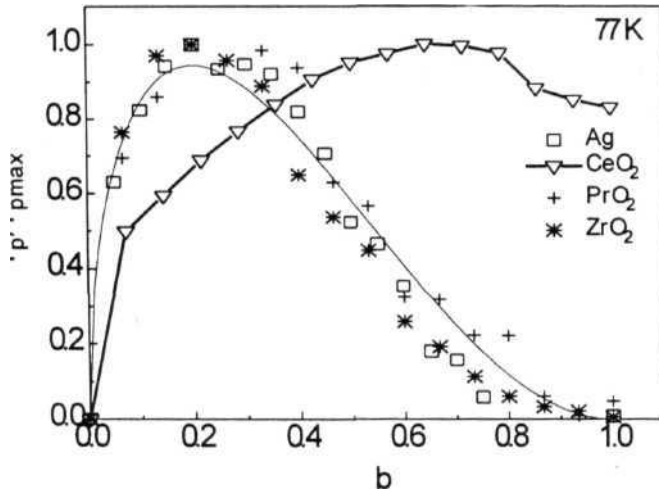
Fig. 4.9 : Plot of the normalized flux pinning force (F_p) vs the normalised field at 77 **K,** for the samples with the additions. The curve is the fitting function, $F_p \propto b^{0.5}(1-b)^2$.

It is observed here that the flux pinning in Sm-123 + 30 mol % can be further increased by the additions of a small amount of any of the additives like CeO_2, PrO_2, ZrO_2 or Ag. All these additions bring about a refinement of the 211 size and probably contribute to additional pinning by increasing the defect density at the 123/211 interface. Of the four additions considered Ag causes the least refinement of 211s, probably because it is in the liquid state at the time of peritectic melting of 123. However, it contributes to the maximum improvement in J_c because it does not react with the parent phase.

A sample of Sm-123 + 10 mol % Sm-211 has a much higher J_c [11], than the Sm-123 + 30 mol % Sm-211 and 0.5 wt % Ag. The high J_c in the former case has been demonstrated a being due to a different pinning mechanism originating from the presence of low-T_c ortho-II phase in the matrix [11]. The evidence for presence of the low-T_c phase in the matrix for Sm-211 concentration from 20 mol % and above was not observable [12]. In the present chapter the Sm-123 + 30 mol % Sm-211 sample is studied, where the contribution to pinning from low-T_c phases is minimal. It will be interesting to explore the possibility of a further increase in J_c of the Sm-123 +10 mol % 211 sample, by refining the 211 particles in the microstructure with the additions like CeO_2, etc.., as the sample has large acicular 211 particles in the microstructure [11].

4.6. CONCLUSIONS

Sm-123 + 30 mol % Sm-211 samples have been melt processed with the additions like CeO_2, PrO_2, ZrO_2 and Ag in the starting material. The microstructures of the samples show a refinement of 211 particles. Amongst the samples, the PrO_2 addition has produced a highly refined microstructure. The starting composition of the sample is Sm-123 with 30 mol % Sm-211. The J_c of the samples has increased incomparison to the sample without these additions. The Ag added sample has the highest J_c among the samples. Samples containing other additions have lower J_c than the Ag added sample, even though the microstructure has a large concentration of fine sized 211 particles. This is due to the non-reactivity of the addition with the parent phase. But the J_c has not reached the value obtained in Sm-123 with 10 mol % 211, where the pinning due to oxygen ordered low-T_c phase predominates (chapter III).

REFERENCES

1. S. Jin, T. H. Tiefel, R. C. Sherwood, R. V. van Dover, M. E. Davis, G. W. Kammlott, and R. A. Fastnacht, Phys. Rev. B 37, (1988) 7850.

2. K. Salama, V. Selvamanickan, L. Gao, and K. Sun, Appl. Phys. Lett 54, (1989)2352.

3. M. Murakami, M. Morita, K. Doi, and K. Miyamoto, Jap. J. Appl. Phys. 28, (1989) L1 125.

4. Z. L. Wang, A. Goyal, and D. M. Kroeger, Phys. Rev. B 47, (1993) 5373.

5. M. Murakami, S.Gotoh, N. Koshizuka, S. Tanaka, T. Matsushita, S. Kambe and K. Kitazawa, Cryogenics 30, (1990) 390.

6. C. J. Kim, K. B. Kim, I. S. Chang, D. Y. Won, H. C. Moon and D. S. Shur, J. Met. Res. 8,(1993)699.

7. C. J. Kim, S. L. Lai, and P. J. McGinn, Mater. Lett. 19, (1994) 185.

8. N. Ogawa, 1. Hirabayashi and S. Tanaka, Physica C 177, (1991) 399.

9. P. J. McGinn, W. Chen, N. Zhu, L. Tan, C. Varanasi and S. Sengupta, Appl. Phys. Lett. 59,(1991)120.

10. L. T. Ramano, O. F. Schilling and C. R. M. Grovener, Physica C 178, (1991) 41.

11. N. V. N. Viswanath and T. Rajasekharan (Communicated).

12. N. V. N. Viswanath and T. Rajasekharan (Communicated).

13. M. Murakami, S. I. Yoo, T. Higuchi, N. Sakai, J. Weltz, N. Koshizuka and S. Tanaka, Japn. J. Appl. Phys. 33, L715, L1000 (1994).

14. D. Shi, S. Sengupta, J. S. Lou, C. Varanasi and P. J. McGinn, Physica C **213,** (1993) 179

15. F. Garcla-Alvarado, E. Moran, M Vallet, J. M. Gonzalez-calbet, M. A. Alario, M. T. Perez-Frias, J. L. Vicent, S. Ferrer, E. Garcia-Michel and M. C. Asensio, Solid. State Comm. 63, (1987) 507.

16. "*Melt Processeed High-Temperature Superconductors*", ed. M. Murakami, World Scientific, Singapore, (1992).

17. M. Mironava, D. F. Lee, and K. Salama, Physica C **211,** (1993) 188.

18. M. Wacenovsky, R. Miltech, H. W. Weber, and M. Murakami, Sup. Sci. & Tech. **4, (1991) S184.**

19. S. Pinol, F. Sandiumenge, B. Martiness, V. Gomis, J. Fohtcuberto, X. Obradors, E. Snoeckand Ch. Roucah. Appl. Phys. Lett. 65, (1994) 1448.

20. E. Sudhakar Reddy and T. Rajasekharan (Communicated)

21. P. O. Hetland. T. H. Johansen, and H. Bratsberg, Cryogenics 36, (1996) 41.

22. D. X. Chen, and R. B. Goldfarb, J. Appl. Phys. 66 (1989) 2489.

23. A. M. Campbell and J. E. Evetts, Physics Reports **21, (1971) 199.**

Table I : The exponents used for fitting the loops to the generalized critical state at 25 K and 77 K.

S.No	Sample	'n' at 25 K	'n'at 77 K
1	Ag	0.3	5
2	CeO_2	0.3	4
3	PrO_2	0.55	6
4	ZrO_2	0.3	8

<u>INFILTERATION GROWTH PROCESS FOR Sm-123</u>

5. 1. INTRODUCTION :

Melt processing of $REBa_2Cu_1O_y$ (123) system results in improved microstructure and current density (J_c) [1-3]. Inspite of these advantages, the melt processed samples however have some inherent defects like shrinkage and macrodefects such as cracks, voids and pores, etc. [4]. Those defects limit the J_c, and also limit making as devices for practical applications. In melt processing, the RE-123 phase is decomposed above its peritectic decomposition temperature, where it incongruently melts into a solid RE_2BaCuO_5 (211) and liquid phases. The surface tension forces exerted by the newly formed liquid shrinks the sample ~ 20-25 %. Moreover, pores and voids form, because of the liquid phase outflow. This melting is accompanied by a change in the dimensions of the sample, which is upto 25% [5]; distortions and cracks may also appear along with the shrinkage.

In ceramic processing techniques like directed metal oxidation (DIMOX) and pressure-less metal infiltration (PRIMEX) [6,7], the molten liquid alloy is allowed to infiltrate or percolate into a semi-porous preform. The advantage of these processing techniques is that large near-net shaped components can be produced, which are free of macro-defects like shrinkage, porosity, etc. The samples need minimal machining after the growth process. On similar lines, recently, a novel processing route has been developed known as the Infiltration-Growth (IG) process [5,8]. In the IG process, the possibility of making near-net shaped high J_c components of Y-123 and Gd-123 superconductors has been

demonstrated. In the **IG** process, a preform of **RE₂BaCuO₅** (RE = Rare earth) is kept in contact with a source of liquid phases and melt processed. In this chapter the extension of that work to the **Sm-123** system is discussed. The Sm-123 system needs to be processed in oxygen-poor atmosphere to reduce the formation of low-T_c solid-solution phases. By processing in reduced oxygen atmosphere the solid-solution formation can be suppressed and the resulting samples will have T_c above 90 K, with high current density [9].

5. 2 EXPERIMENTAL DETAILS

The precursor powders were prepared by solid-state sintering route. The **Sm-211** and **Sm-123** powders were prepared by taking required amounts of Sm_2O_3, $BaCO_3$ & CuO and mixing them thoroughly in a centrifuge mill using an organic liquid as the medium. The dried powders were sintered at 975°C and **930°C** to form **Sm-211** and Sm-123, respectively. The sintering was repeated twice to achieve phase purity. Two different configurations were tried for the IG process. In one configuration the **Sm-211** preform was kept below the 123 pellet, in this configuration the liquid will infiltrate into the 211 preform at the high temperature melting and the usual growth process of 123 takes place. In a second configuration the 211 preform was kept above the 123 pellet and the usual melt processing was done. In the second process named as IG-2, the liquid will percolate into the 211 preform based on the capillary action and the growth of 123 will take place. These were melt processed by melting at 1115°C for 10 minutes, and then slow cooled from 1060°C to 950°C at a rate of 1°C/hr, all under flowing Argon gas. The

samples were oxygenated in flowing oxygen atmosphere according to the schedule described in the experimental chapter.

5.3. PRELIMINARY CHARACTERISATION

The X-ray diffraction patterns (Fig. 5.1) of the two samples showed the formation of the Sm-123 phase with some amount of Sm-211. The lattice parameter values matched that reported for Sm-123 values [10], indicating that the solid-solution formation has been suppressed to a large extent. The T_cs (Fig. 5.2) of the samples were above 90 K, confirming that the solid-solution formation had been suppressed to a large extent. During the melt processing the Sm-123 melted and the liquid infiltrated the Sm-211 preform. Slow cooling through T_p produced void-free specimens (as seen from cutting the samples), with large domains of 123 visible to the naked eye. The dimensions of the samples of the samples showed no change after melt processing.

5.4. MICROSTRUCTURAL FEATURES

Samples were quenched just after melting at 115oC to study the infiltration of the liquid phases into the Sm-211 preform. Fig. 5.3 shows the typical microstructure of a quenched sample using an SEM. The particles appearing white are the Sm-211 phase, and the black background is the liquid phase. The SEM image shows that the liquid phases completely fill the vacant regions between the blocky Sm-211 particles. The ease with which complete infiltration has occurred without the application of an additional driving force like pressure encourages from the view point of fabricating large samples with the 1G process. The particle size of
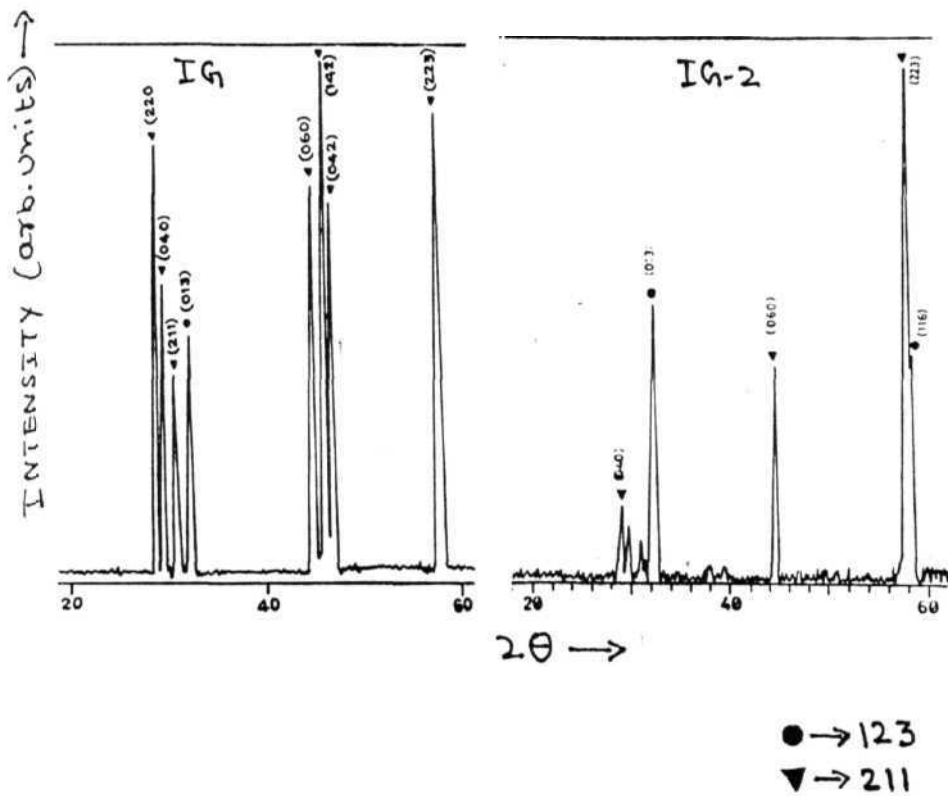
Fig. 5.1 : XRD patterns of the IG processed samples showing the presence of Sm-123 and Sm-211 phases.
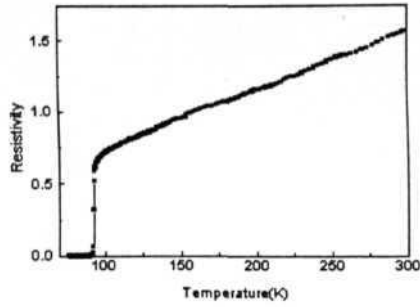
Fig. **5.2(a)**: Resistivity vs temperature plot of the IG processed sample. The T_c of the sample is 90.4 **K**.
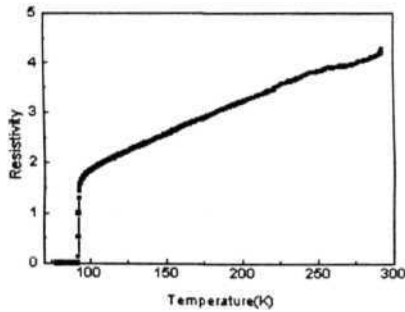

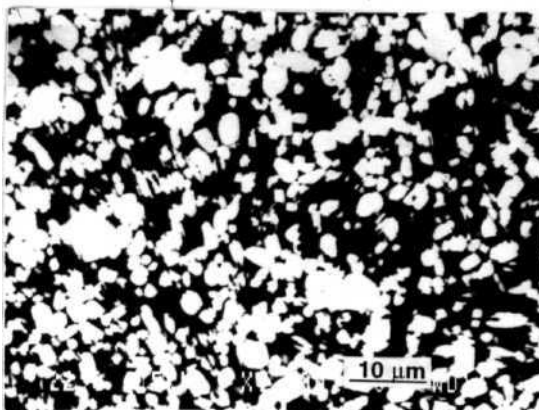Fig. **5.2(b)**: Resistivity vs temperature plot of the IG-2 processed sample. The T_c of the sample is 90.1 K.

Fig. 5.3 : SEM image of the sample quenched after the infiltration of liquid phases into the Sm-211 preform.
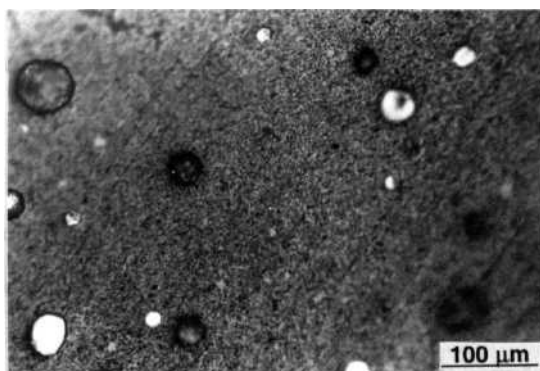

Fig. 5.4 : Optical micrograph of the IG processed sample indicating less porosity in

the sample.

the Sm-211 in the liquid is very small and there has not been a large coarsening of such particles in the liquid. Fig. 5.4 shows the optical micrograph of the as polished melt processed sample. The micrograph shows a uniform distribution of the Sm-211 particles. The uniformity of distribution and the possibility of tailoring the 211 size is an advantage with the process. Also, the sample has less porosity and voids, due to the reasons mentioned above. Fig. 5.5 is an SEM image at higher magnification. The average size of the Sm-211s in the textured samples is approximately 1 urn. Fig. 5.6 is a fractured surface of the sample, which shows parallel Sm-123 grains in the sample. Fig. 5.7 is the SEM image of the sample prepared by a second configuration (1G-2) in which the Sm-211 preform is kept above the source of liquid phases. The liquid phases move up into the Sm-211 preform by the capillary action. Similar features are seen in this sample as seen in Fig. 5.5. From the SEM images the volume percentage of the 211 particles occupied in the microstructure is evaluated using standard metallographic techniques [11]. The volume percentage is ~ 70 % in both the samples, this corresponds to a sample with starting composition of Sm-123 with 40 mol % Sm-211 for melt processing. This conclusion is arrived on the basis of the data from the micrographs of melt processed Sm-123 with increasing concentrations of Sm-211 (0 to 40 mol % Sm-211, chapter III), where the features like platelet width and gap width match that of the 1G processed samples. However, the difference in the IG sample is that the 211 particles are highly refined in the microstructure, where as, in conventionally melt processed sample of Sm-123 with 40 mol % of Sm-211, the 211 particles are much larger in size.
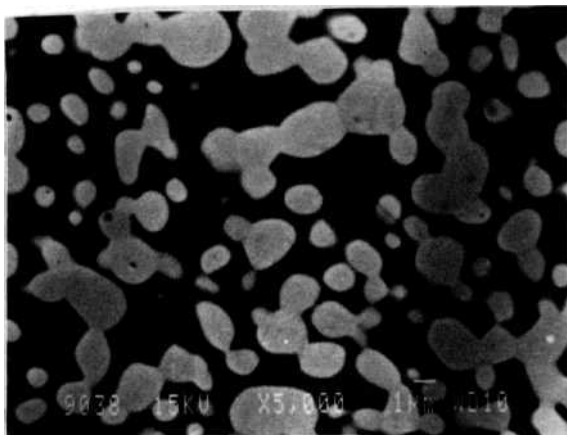
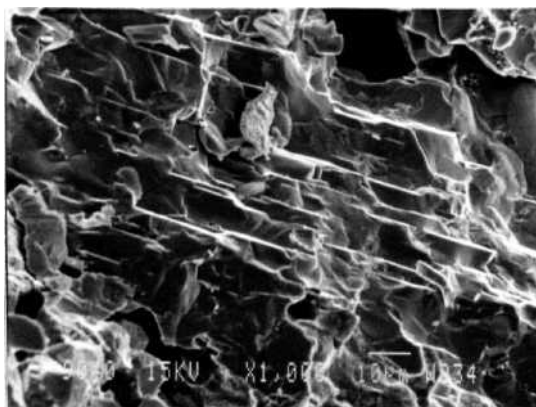Fig. 5.5 : SEM image of the IG processed sample showing the usual features of melt processed samples.

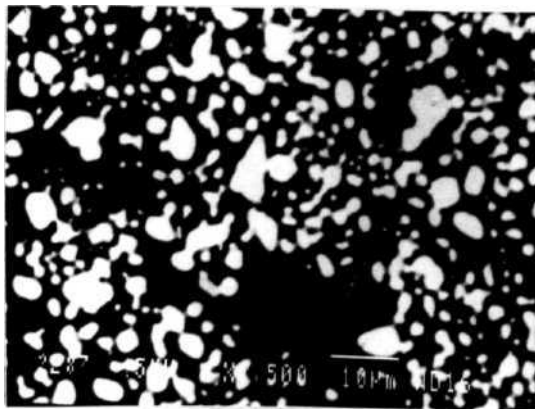Fig. 5.6 : SEM image of the fractured surface of IG processed sample showing the aignment of the grains.

Fig. 5.7 : SEM image of the IG-2 processed sample having similar features as the IG processed sample.

5.5. CURRENT DENSITY

The dc magnetic hysteresis (M-H) loops recorded at 5 K, 35 K & 77 K, for field applied normal to the sample surface are shown in Fig. 5.8. No anomalous features like peak-effect were present, as observed in the stiochiometric RE-123 melt processed samples [13,14].
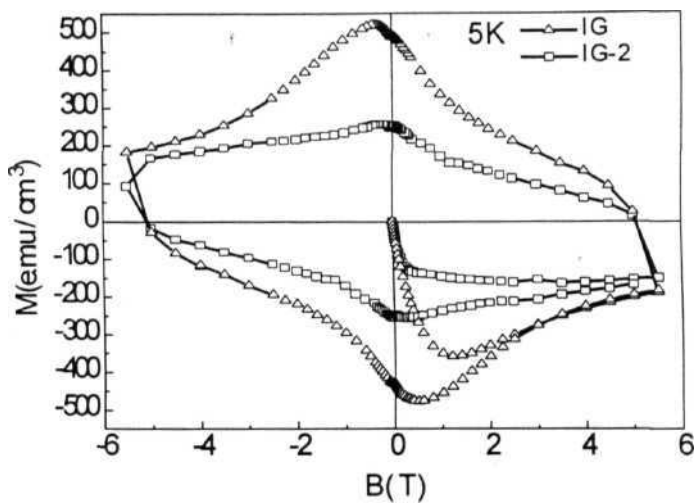
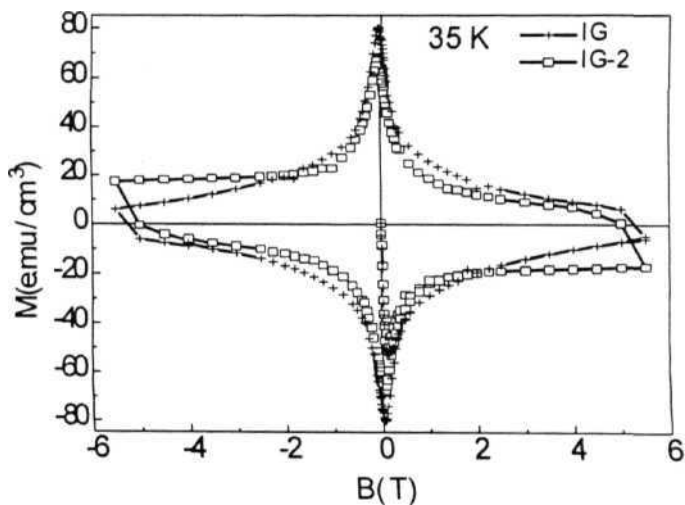Fig. 5.8(a). : M-H loops of the IG processed samples at 5 K.

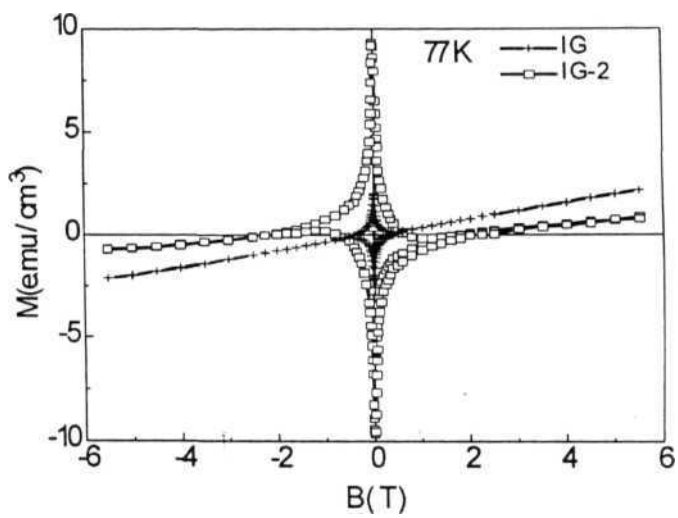Fig. 5.8(b). : M-H loops of the IG processed samples at 35 K.

Fig. 5.8(c). : M-H loops of the IG processed samples at 77 K.

The J_c is evaluated using the Beans critical state model from the loops recorded at various temperatures, is plotted in Fig. 5.9, against the field. The flux pinning force was calculated using the relation, $F_p = J_c B/10$. The data at 77 K are plotted in Fig. 5.10, which clearly shows that the IG sample has a higher pinning force. The variation of the normalised pinning force (F_p/F_{pmax}) with the normalised field b (B/B*, B*= max. field) is plotted in Fig. 5.11. The two samples have a peak around 0.2 [15].
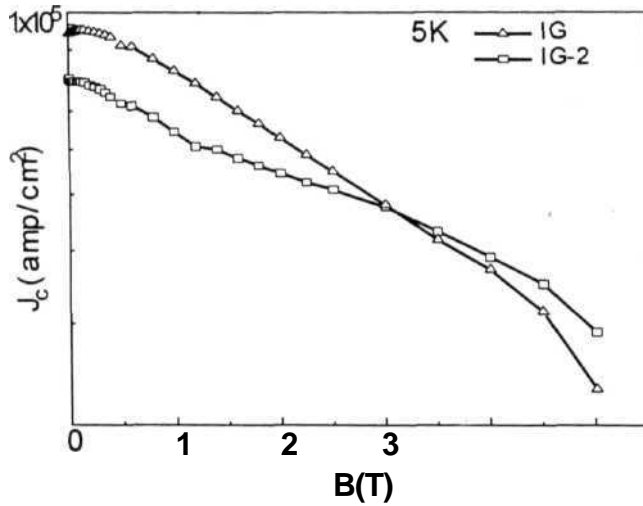

Fig. 5.9(a). : J_c vs B plots of the samples at 5 K.
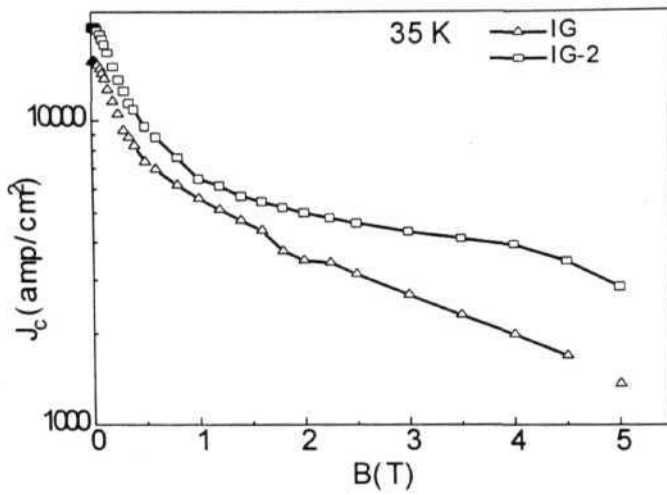
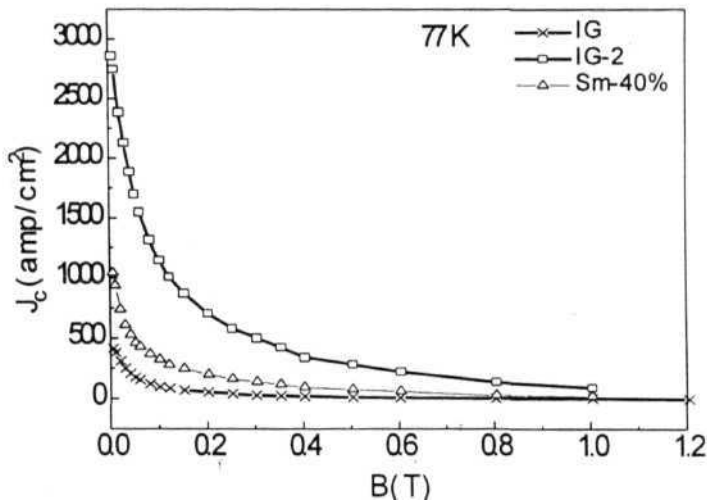Fig. 5.9(b). : J_c vs B plots of the samples at 35 K.

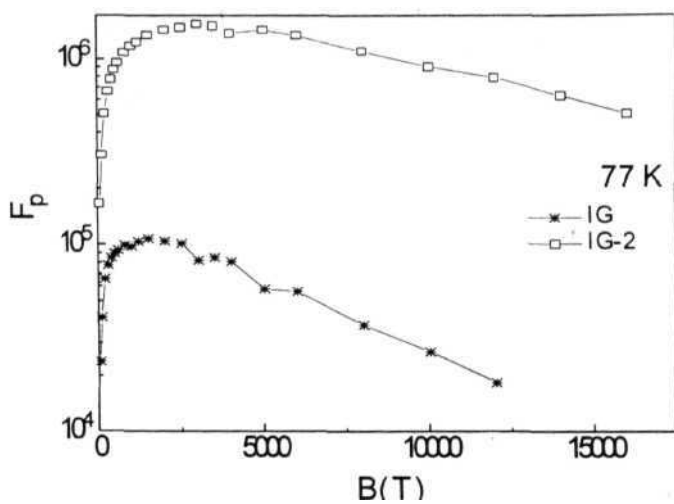Fig. S.9(c). : J_c vs B plots of the samples at 77 K.

Fig. 5.10 : Plot of the variation of the pinning force with field at 77 K.
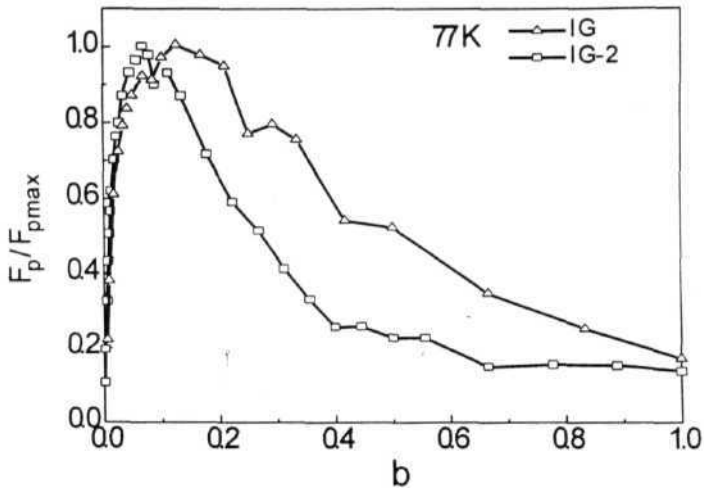
Fig. **5.11** : Plot of the variation of the normalized pinning force with normalized field at 77 K.

5.6. IRREVERSIBILITY LINE

The irreversibility line is for the IG processed sample is plotted in Fig. 5.12. The IR line is less steeper in comparison to the samples showing high J_c in the Sm-123 system, indicating that the pinning strength of the sample is low. This can also be shown from Fig. 5.10. The IR line has a slope change at a field around 0.4 Tesla.

5.7. MAGNETIC RELAXATION

The magnetic relaxation rate of the sample is measured at a lower temperature. Fig. 5.13 shows the variation of the normalized relaxation rate with field at 30 K. The relaxation rate initially decreases upto a field of 0.3 Tesla and later increases with field, but the relaxation rate has a slope change at a field of 2.8

Tesla. In Fig. 5.14, the J_c, flux pinning force and the relaxation rate are plotted together against the field. The J_c decreases and the relaxation rate increases with field. The flux pinning force has a peak in the 2-3 Tesla region. It is known that, the behaviour of the J_c in superconductors is dominated by pinning in the low fields and by the relaxation rate in high fields [16]. In the IG processed sample such similar
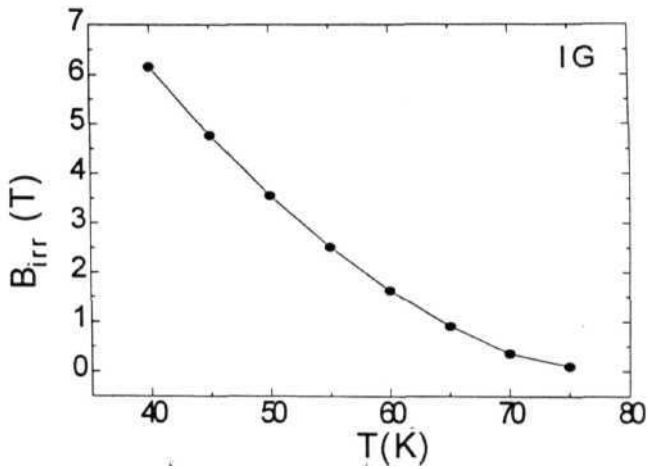

Fig. 5.12 : Irreversibility line of the IG processed sample for H parallel to c-axis.
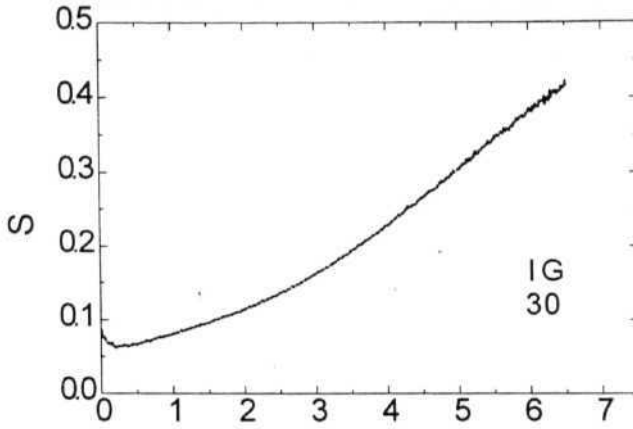
Fig. 5.13 : Variation of the relaxation rate with applied field at 30 K for the IG processed
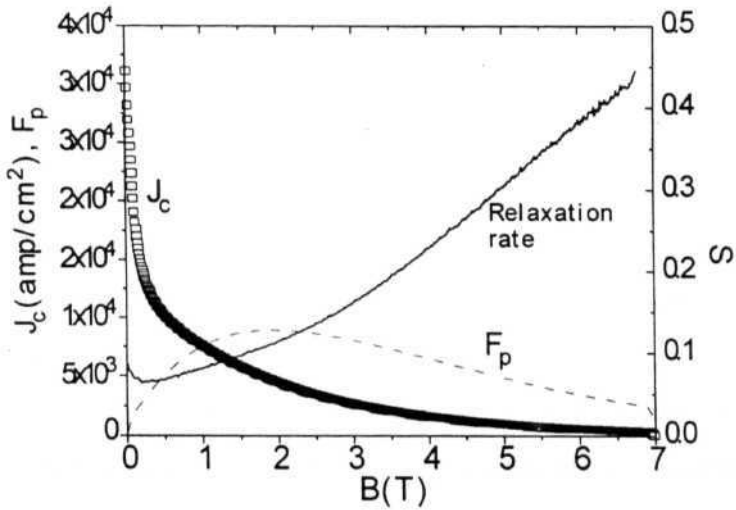sample.

Fig. 5.14 : Comparative plot J_c, flux pining force (F_p) and relaxation rate (S) against the applied field at 30 K.

effect is observed. The creep rate has a slope change at a field above the point at which the flux pinning force has a peak. This indicates the pinning force saturates at the peak value, and above that field, relaxation rate will dominate the properties.

5.8. CONCLUSIONS

The aim of this work was to demonstrate that the IG process is a viable way of melt processing Sm-123 phase with good microstructural features. There is an improvement in the refinement of Sm-211 inclusions, but the J_c is not very high. It is proposed that the low J_c in the IG processed Sm-123 sample is primarily due to the large volume percentage of Sm-211 in the microstructure. The J_c dependence in the Sm-123 melt processed samples on increasing Sm-211 content has been found to have two peaks (chapter III, Fig. 3.14) [12]. A major peak exists at the 10 mol % Sm-211 concentration, and a minor peak at 30 mol %. As discussed in chapter III, low at concentrations of 211, an additional field induced pinning from the low-T_c oxygen deficient regions helps to enhance the J_c. For increasing 211 content (above 20 mol %), the field induced pinning is absent, and the J_c decreases [14]. This is unlike in the Y-123 and Gd-123 [17,18] systems where the maximum in Jc as a function of 211 concentration occurs at - 30 mol % of 211. In these systems the predominate contribution to the pinning comes form the defects at the 123/211 interface.

It is proposed that, in the present IG samples the relatively high concentration of Sm-211 has suppressed the spinodal transformation (chapter III) and the pinning in it is predominantly from the 123/211 interface defects. The pinning from such interfaces does not contribute to J_c enhancement substantially

in the LRE-123 systems as is evident from the present experiments (chapter III) and the work of others [19].

Because of the dramatic advantages of possible shape forming in combination with J_c enhancement by the IG process, it is highly desirable to enhance the J_c further in IG processed Sm-123. A possible way of doing as suggested by the present work is to reduce the Sm-211 content in the microstructure.

REFERENCES :

1. S. Jin, T. H. Tiefel, R. C. Sherwood, R. V. van Dover, M. E. Davis, G. W. Kammlott, and R. A. Fastnacht, Phys. Rev. B 37, (1988) 7850.

2. K. Salama, V. Selvamanickan, L. Gao, and K. Sun, Appl. Phys. Lett 54, (1989)2352.

3. M. Murakami, M. Morita, K. Doi, and K. Miyamoto, Jap. J. Appl. Phys. 28, (1989) L1 125.

4. M. Murakami, Critical Currents & Processing of Melt Textured Materials, World Scientific, Singapore.

5. E. Sudahakar Reddy and T. Rajasekharan **(J. Mater. Res.** in Press).

6. A. W. Urquhart, Mater. Sci. Engg. A **144** (1991) 75.

7. A. S. Naelberg, J. Mater. Res, 7 (1992) 265.

8. T. Rajasekharan, E. Sudhakar Reddy , Proc. of the ASMCCD Symp., Mumbai, INDIA, 1996 (in press).

9. S. I. Yoo, M. Murakami, T. Higuchi, N. Sakai, J. Weltz, N. Koshizuka and S. Tanaka, Jpn. J. Appl. Phys. 33, (1994) L715.

10. F. Garcla-Alvarado, E. Moran, M. Vallet, J. M. Gonzalez-calbet, M. A. Alario, M. T. Perez-Frias, J. L. Vicent, S. Ferrer, E. Garcia-Michel and M. C. Asensio, Solid. State Comm. 63, (1987) 507.

11. *Interpretation of Metallographic Structures,* W. Rostoker, Acad. Press., P.213.

12. N. V. N. Viswanath, T. Rajasekharan, L. Menon, N. H. Kumar, S. K. Malik, G. K. Dey, D. D. Upadhyaya (Communicated).

13. M. Murakami, S. I. Yoo, T. Higuchi, N. Sakai, J. Weltz, N. Koshizuka and S. Tanaka, Jpn. J. Appl. Phys. 33, (1994) L1000.

14. N. V. N. Viswanath, T. Rajasekharan, L. Menon, N. H. Kumar. S. K. Malik, G. K. Dey, D. D. Upadhyaya (Communicated).

15. A. M. Campbell and J. E. Evetts, Phys. Reports 21, (1971) 199.

16. Y. Yeshrun, A. P. Malozemoff, A. Shaulov, Rev. Mod. Phys. 68, (1996) 911.

17. M. Muralkami, S. Gotoh, N. Koshizuka, S. Tanaka, T. Matsushita, S. Kambe, and K. Kitazawa, Cryogenics 30, (1990) 390.

18. E. Sudahakar Reddy and T. Rajasekharan (Phys Rev. B. in Press).

19. R. Yu, F. Sandiumenge, B. Martinez, N. Vilalta and X. Obrados, Appl. Phys. Lett. 71,(1997)413.

CHAPTER VI

CONCLUSIONS

The microstructure and J_c behaviour of melt processed Sm-123 system is studied with increasing Sm-211 concentration in the starting material. It is observed that, for low concentration of 211 in the starting material, the 211 particles in the microstructure have acicular morphology. With increase in 211 concentration, the morphology changes to spherical. A sudden change in the microstructural features above 10 mol % Sm-211 concentration is observed. The 211-free regions formed in the microstructure is explained as due to the in-homogeneities occurring in the 2-phase mixture above T_p due to acicularity of the 211 particles in the mixture. Such an explanation is consistent with the size of the 211-free regions decreasing in the same manner with increasing 211 content, as do the size of acicular 211 particles. With increase in 211 concentration from 0 to 10 mol %, the J_c increases. .

A TEM study of the 10 mol % sample shows evidence of a transformation in the images, and also the presence of crystallographic defects like stacking faults, dislocations, etc. The SAD pattern of the transformed region shows the presence of ortho-II regions (T_c - 60 K). The low-T_c ortho-II phase can be the source of field induced pinning contributing to the increase in J_c of the material, even though the 211 particles are acicular and have a large size. Increasing the 211 content to 20 mol % decreases the J_c by a large amount, and the evidence of the transformation and defects are not present in the TEM images. At a 211 concentration of 30 mol

%, the J_c has a minor peak. In the melt processed **Y-123** or **Gd-123** system, the J_c is maximum at 30 mol % 211 concentration. It has been reported in the literature by a TEM study of elliptical 211 inclusions that, **crystallographic** defects appear in the 123 matrix at 123/211 interface below a critical size. The crystallographic defects enhance the J_c of the material. Like at the 30 mol % 211, the 211 inclusions in the **Sm-123** sample are of a fine size, and the minor peak in J_c at 30 mol % 211 can have its origin in the pinning of the flux by secondary defects around the 211 inclusions. However, the J_c in that sample is not as high as in the **Y-123** or Gd-123 sample with similar 211 content. Beyond 30 mol % of 211, the microstructural features saturate and the J_c decreases for further increase in 211 due to a reduction in the superconducting matrix. It appears that behavior of **RE-123** samples can be grouped into two with respect to their dependence of Jc on the concentration of 211 inclusions : the **LRE-123** samples with a rare earth atom like Nd, **Sm,** have a peak near 10 mol % of 211; and **RE-123** systems with atoms like Y and Gd the peak is at 30 mol % 211 concentration.

Melt textured Sm-123 samples with (10 mol %) and without **Sm-211** addition have been studied using a VSM form low temperatures to 90 **K** and upto fields of 6 T. The two samples exhibit an anomalous peak-effect in the magnetization hysteresis loop. The Sm-123 sample with 10 mol % **Sm-211** exhibits a pronounced peak effect and the stoichiometric sample has a moderate effect. TEM measurements on the samples identified the origin of the peak effect, which is due to the field induced pinning from **low-T_c** oxygen deficient 123 regions in the sample distributed on a nanometer scale. The temperature variation of the hysteresis loops indicate the same, because the peak position in the loops shifts to

low fields with the increase in temperature. The J_c of the first sample is high in the temperature ranges where the peak-effect is predominant. In other temperatures the second sample is having, the higher J_c. The IR line for the first sample is found to be much steeper incomparison to the second sample, indicating that the pinning strength in it is higher. Relaxation rate measured as a function of field at 77 K shows that for the second sample it initially decreases with field to a low value and then increases at high fields. The field at which the minimum in relaxation rate is observed is not coincident with the field at which the peak in the J_c or the loop exists. This indicates that the peak in the M-H loop is not due to a drop in the relaxation rate. The peak is primarily due to the field induced pining.

Sm-123 + 30 mol % Sm-211 sample was melt processed with the additions like CeO_2, PrO_2, ZrO_2 and Ag, in the starting material. This was done to refine the Sm-211 particles in the microstructure and to study the effect on J_c. The microstructures of the samples show a refinement of 211 particles. Amongst the samples, the PrO_2 addition has produced a highly refined microstructure. The J_c of the samples has increased in comparison with the sample without these additions. The Ag added sample has the highest J_c among the samples. Samples containing other additions have lower J_c than the Ag added sample, even though the microstructure has a large concentration of fine sized 211 particles. This is due to the non-reactivity of Ag addition with the parent phase.

Melt textured samples of Sm-123 was prepared by following a novel method of Infiltration-Growth process. This was done with an aim to process the samples free of macro-defects and to observe the J_c behaviour. It is observed that the IG processed samples were free of any macro-defects and have good

133

microstructural features like freedom from porosity, a good degree of texturing and very fine size 211 particles. The overall J_c of the samples is however low, because of the presence of large volume of 211 particles in the microstructures. The J_c of samples with high 211 concentration was found to be low, because of the absence of low-T_c field induced pinning and low contribution towards pinning form the 123/211 interface defects in the LRE-123 systems, unlike in RE-123 systems where the contribution from interface pinning will be predominant.

LIST OF PUBLICATIONS :

1) "ORIGIN OF PEAK EFFECT IN THE MAGNETIZATION HYSTERESIS LOOP OF MELT PROCESSED $RE_1Ba_2Cu_3O_y$ SUPERCONDUCTORS"

N. V. N. Viswanath, T. Rajasekharan, Latika Menon, N. Harish Kumar,

S. K. Malik, G. K. Dey, and D. D. Upadhyaya,

Applied Physics Letters (In Press).

2) "REFINEMENT OF INSULATING Sm_2BaCuO_5 PHASE AND ITS EFFECT ON

J_c IN MELT PROCESSED $SmBa_2Cu_3O_y$ SYSTEM"

N. V. N. Viswanath and T. Rajasekharan
Physica C (In press)

3) EFFECT OF Sm_2BaCuO_5 ADDITION ON THE PROPERTIES OF MELT PROCESSED $SmBa_2Cu_3O_y$

N. V. N. Viswanath and T. Rajasekharan, Latika Menon, N. Harish Kumar, S. K. Malik, G. K. Dey and D. D. Upadhyaya

Communicated

4) "PEAK-EFFECT, IRREVERSIBILITY LINE & RELAXATION RATE OF MELT TEXTURED Sm-123"

N. V. N. Viswanath and T. Rajasekharan, and Hienz. Kupfer

Communicated.

5) "INFILTRATION-GROWTH PROCESSING OF $SmBa_2Cu_3O_y$ SUPERCONDUCTOR"

N. V. N. Viswanath, T. Rajasekharan, N. Harish Kumar, L. Menon and S. K. Malik

Communicated.